A periplasmic L,D-carboxypeptidase is important for cell morphology, membrane integrity, and virulence in *Francisella tularensis*

Briana Zellner[1], Dominique Mengin-Lecreulx[2], William T. Gunning 3rd[3], Robert Booth[3], Jason F. Huntley[1*]

[1] Department of Medical Microbiology and Immunology, University of Toledo, Toledo, OH, U.S.A.; [2] Institute for Integrative Biology of the Cell (I2BC), CEA, CNRS, Univ. Paris-Sud, Université Paris-Saclay, 91198 Gif-sur-Yvette, France; [3]Department of Pathology, University of Toledo, Toledo, OH, U.S.A.

Running Head: *F. tularensis* L,D-carboxypeptidase

To whom correspondence should be addressed: Jason F. Huntley, Department of Medical Microbiology and Immunology, University of Toledo College of Medicine and Life Sciences, 3000 Arlington Ave., MS1021, HEB 200D, Toledo, OH, U.S.A., 43614. Tel.: 419-383-5456; Email: Jason.Huntley@UToledo.edu

Abstract word count: 192

Text word count: 9082

Abstract

F. tularensis is a Gram-negative, intracellular bacterium that causes the zoonotic disease tularemia. Intracellular pathogens, including *F. tularensis*, have evolved mechanisms to allow survival in the harsh environment of macrophages and neutrophils, where they are exposed to cell membrane-damaging molecules. One mechanism that protects intracellular Gram-negative bacteria from macrophage or neutrophil killing is the ability to recycle and repair damaged peptidoglycan (PG), – a process that requires over 50 different PG synthesis and recycling enzymes. In addition to PG repair, PG recycling occurs during cell division and plays critical roles in maintaining cell morphology, structure, and membrane integrity. Here, we identified a PG recycling enzyme, L,D-carboxypeptidase A (LdcA), of *F. tularensis* that is responsible for converting PG tetrapeptide stems to tripeptide stems. Unlike prototypic LdcA homologs, *F. tularensis* LdcA is outer membrane-associated and also exhibits L,D-endopeptidase activity, converting PG pentapeptide stems to tripeptide stems. Loss of *F. tularensis* LdcA led to altered cell morphology and membrane integrity, as well as attenuation in a mouse pulmonary infection model and in primary and immortalized macrophages. Finally, a *F. tularensis* LdcA mutant protected mice against virulent Type A *F. tularensis* SchuS4 pulmonary challenge.

Importance: PG is well known to play important roles in protecting bacteria from external insults and osmotic stress. However, pathogenic bacteria modify their PG architecture to avoid antibiotic activity and/or encode PG recycling and repair pathways to promote bacterial virulence. Prototypic Gram-negative bacteria, including *E. coli* and *Pseudomonas aeruginosa,* recycle PG in a multi-enzyme pathway, including the cytoplasmic L,D-carboxypeptidase, LdcA. Here, we demonstrated that a previously unstudied protein from the intracellular bacterium *F.*

tularensis contains an LdcA conserved domain, this *F. tularensis* LdcA is outer membrane-associated, and deletion of this LdcA ortholog increases bacterial outer membrane thickness, resulting in bacteria that are more resistant to various stressors (e.g., H_2O_2, NaCl, low pH), yet are completely attenuated in a mouse pulmonary infection model. Finally, we demonstrated that the *F. tularensis* LdcA mutant can be used as a live, attenuated vaccine to protect against pulmonary challenge with fully virulent *F. tularensis.*

Keywords: Tularemia, peptidoglycan, L,D-carboxypeptidase, virulence, *F. tularensis*

Introduction

The Gram-negative bacterial cell wall plays an important role in maintaining cell shape, protecting against external insults, and preventing cell lysis amid fluctuations in internal turgor pressure (1). The cell wall is composed of peptidoglycan (PG), a network of alternating *N*-acetylglucosamine (GlcNAc) and *N*-acetylmuramic acid (MurNAc) glycan chains that are crosslinked through peptide stems, and lies just outside of the cytoplasmic membrane of most bacteria (2, 3). PG has been shown to be covalently attached to the outer membrane (OM) of Gram-negative bacteria by Braun's lipoprotein, and noncovalently attached by Pal and other lipoproteins (4-7). A loss of membrane integrity can occur if interactions between PG and attached lipoproteins are disturbed, thus it is extremely important to maintain correct PG architecture.

Synthesis of Gram-negative PG precursors, studied mainly in *E. coli*, occurs in the bacterial cytoplasm and requires a series of enzymes to build a pentapeptide PG monomer before moving this molecule into the periplasm. Periplasmic PG cross-linking most often occurs between the fourth residue (D-Ala) of newly formed pentapeptide stems to the third residue (*meso*-A_2pm) of existing tripeptide stems (4-3 cross links), resulting in the release of the pentapeptide terminal D-Ala and forming tetrapeptide stems (8, 9). As new PG is formed and incorporated, older layers of PG must be cleaved to maintain consistent sacculus thickness (10). Up to 60% of PG is recycled per generation, which repairs damaged PG and also provides energy during periods of stress or starvation (1, 11, 12). Together, there are more than 50 different enzymes, mostly cytoplasmic, involved in Gram-negative PG synthesis and recycling. PG homeostasis is extremely important, as mutations in any one of these enzymes can result in altered cell morphology, changes in cell membrane integrity, and reduced ability to replicate and

divide (1). Importantly, a recent review highlighted the largely neglected field of Gram-negative bacterial PG synthesis and recycling, particularly given the growing threat of antimicrobial resistance and association of PG homeostasis with virulence (13). For example, *Acinetobacter baumannii* penicillin-binding protein (PBP) mutants were unable to survive *in vitro* or *in vivo* and were more sensitive to complement-mediated killing than wild-type bacteria (14) and *Helicobacter pylori* PG hydrolase (AmiA) mutants were unable to colonize mouse stomach tissue (15).

PG recycling, mainly characterized in *E. coli*, begins with periplasmic lytic transglycosylase (LT) cleavage of the β-1,4-glycosidic linkage between MurNAc and GlcNAc, forming a GlcNAc-1,6-anhydro-MurNAc product, which allows for either insertion of new muropeptides or recycling of GlcNAc-1,6-anhydro-MurNAc (16). Low molecular mass penicillin binding proteins (LMM PBPs) can function as endopeptidases, cleaving the cross-links between adjacent tetrapeptide stems, and/or as D,D-carboxypeptidases, removing the terminal D-Ala of pentapeptides during transpeptidation (cross-linking) reactions, forming the tetrapeptide [1, 20]. Amidases then remove the tetrapeptide stems from GlcNAc-1,6-anhydro-MurNAc, the peptide stems and GlcNAc-1,6-anhydro-MurNAc are transferred into the cytoplasm via inner membrane permeases, and cytoplasmic L,D-carboxypeptidases (Ldc) cleave the terminal D-Ala from the tetrapeptide, resulting in a tripeptide, and allowing for additional hydrolases to further degrade PG [1]. PG is unusual in that it is both highly dynamic (*e.g.*, allowing for bacterial division and molecular transport across the periplasm), yet tightly regulated to prevent membrane collapse and bacterial death. As such, PG recycling enzymes have been speculated to be important virulence determinants in Gram-negative bacteria [30]. Indeed, *E.coli* Ldc mutants lyse in stationary phase [26] and are more susceptible to β-lactam antibiotics [27], *Helicobacter*

and *Campylobacter* Ldc mutants have altered cell morphology [28, 29] and defects in motility and biofilm formation [28], and *Neisseria gonorrhoeae* Ldc mutants are unable to stimulate NOD1-dependent responses in the host [66]. However, very little is known about the importance of PG recycling enzymes in the pathogenesis of intracellular pathogens such as *Francisella tularensis*.

F. tularensis, the causative agent of tularemia, is a Gram-negative, intracellular, coccobacillus that can infect and cause lethal disease in many species, including humans (17, 18). There are three subspecies of *F. tularensis*, subsp. *tularensis* (Type A), subsp. *holarctica* (Type B), and subsp. *mediasiatica*, although only subsp. *tularensis* and subsp. *holarctica* are virulent for humans (19). *F. tularensis* poses a severe threat to public health and has been classified as an NIH Category A Priority Pathogen and a CDC Tier 1 Select Agent due to its low infectious dose (<10 CFU), ease of aerosolization, and high morbidity and mortality rates (up to 60%) (20, 21). Like other intracellular pathogens, *F. tularensis* has evolved different mechanisms to infect, survive, and replicate within host cells, including macrophages and neutrophils (22). However, this lifestyle exposes the bacteria to reactive oxygen species (ROS), reactive nitrogen species (RNS), antimicrobial peptides, and other cell membrane- and cell wall-damaging molecules (23). Our group previously demonstrated that the *F. tularensis* disulfide bond formation protein A (DsbA) ortholog repairs damaged outer membrane proteins and known virulence factors. We additionally showed that *F. tularensis* DsbA, unlike periplasmic DsbA in *E. coli* and most other Gram-negative bacteria, is outer membrane-bound and is a multifunctional protein with both oxidoreductase and isomerase activities. Finally, using a molecular trapping approach, we identified over 50 *F. tularensis* DsbA substrates, many of which we speculate are involved in virulence (24).

Here, we determined the function of one of those *F. tularensis* DsbA substrates – a previously unstudied hypothetical protein containing a putative LdcA domain – and assessed its role in bacterial virulence. Deletion of *F. tularensis* LdcA resulted in bacteria with altered cell morphology, increased sensitivity to β-lactam antibiotics, yet increased resistance to several stressors (*e.g.*, H_2O_2, NaCl, low pH). Next, we demonstrated that *F. tularensis* LdcA exhibits L,D-carboxypeptidase and L,D-endopeptidase activities on pentapeptide and tetrapeptide residues of PG. Finally, we established that *F. tularensis* LdcA is required for virulence, as mutants were unable to replicate in macrophages or cause disease in mice.

Results

FTL1678 contains a putative L,D-carboxypeptidase domain

Previous studies by our group and others have shown that *F. tularensis* DsbA mutants are attenuated in mice (25). However, additional work by our group, demonstrating that DsbA possesses both oxidoreductase and isomerase activities to repair damaged envelope and cell membrane proteins, indicated that other envelope proteins likely are responsible for *F. tularensis* virulence (24). To identify new *F. tularensis* virulence factors, we used a molecular trapping approach and identified over 50 *F. tularensis* DsbA substrates (24). One of those DsbA substrates, FTL1678, is annotated in the *F. tularensis* genome as a conserved membrane hypothetical protein. Here, a conserved domain search revealed that a large portion of FTL1678 contains a putative Ldc domain, part of the peptidase_S66 superfamily (Fig. S1). Ldc proteins have been studied in a number of Gram-negative bacteria, including *E. coli* (26-29), *Pseudomonas aeruginosa* (30), *N. gonorrhoeae* (31), and *Campylobacter jejuni* (32). To further explore this conserved domain, amino acid sequences of FTL1678 (*F. tularensis* subsp.

holarctica [Type B] LVS) and FTT0101 (homolog of FTL1678 in *F. tularensis* subsp. *tularensis* [Type A] SchuS4) were aligned with LdcA orthologs from *E. coli*, *P. aeruginosa*, *N. gonorrhoeae*, and *C. jejuni* (named Pgp2). Despite low percentages of amino acid identities among the LdcA orthologs (6.3% to 30.3%; Fig. 1), there was a higher degree of amino acid similarity among LdcA orthologs (13.0% [*E. coli* and *C. jejuni*] to 44.7% [*E. coli* and *N. gonorrhoeae*]; Fig. 1). Notably, the LdcA Ser-Glu-His catalytic triad, previously shown to be required for *P. aeruginosa* LdcA activity (30), was absent from *C. jejuni* Pgp2 but was present in all LdcA homologs, including FTL1678 and FTT0101 (Fig. 1).

E. coli and *P. aeruginosa* Ldcs have been localized to the bacterial cytoplasm (27, 30, 33). However, *C. jejuni* Pgp2 is unusual in that it contains a signal peptide and has been speculated to be periplasmic (32). In addition, *N. gonorrhoeae* LdcA was found to be periplasmic and outer membrane-associated (31). As noted above, we previously demonstrated that FTL1678 is a DsbA substrate (24), indicating that FTL1678 is located in the *F. tularensis* envelope (*i.e.*, in the inner membrane [IM], periplasm, or outer membrane [OM]). Bioinformatic analyses of FTL1678 indicated that it is a periplasmic protein due to the presence of a signal peptide but absence of OM or lipoprotein signatures (Table S3). To experimentally confirm FTL1678 localization, we generated an *F. tularensis* strain with 6× histidine-tagged FTL1678, then performed spheroplasting, osmotic lysis, and sucrose density gradient centrifugation to separate IM and OM fractions and probe for protein subcellular localization. Immunoblotting of whole-cell lysates (WCL), OM fractions, and IM fractions demonstrated that the OM control protein, FopA (34), only was present in WCL and OM fractions (but not IM fractions; Fig. 2) and the IM control protein, SecY (34), only was present in WCL and IM fractions (but not OM fractions; Fig. 2). By comparison, FTL1678 only was detected in WCL and OM fractions,

demonstrating OM-association and indicating that FTL1678 may be periplasmic. To further explore this possibility, we examined localization of the periplasmic protein TolB, which is well-known in Gram-negative bacteria to bind PG with the peptidoglycan associated lipoprotein, Pal (35, 36). Notably, we previously demonstrated that *F. tularensis* Pal is OM-localized (34) , similar to other Gram-negative bacteria. Here, *F. tularensis* TolB was detected in OM fractions, but not IM fractions, confirming its OM-association and providing further evidence that FTL1678 is OM-associated and may be a periplasmic protein (Fig. S2).

FTL1678 exhibits L,D-carboxypeptidase and L,D-endopeptidase activities

To confirm the predicted Ldc domain in FTL1678 and FTT0101, recombinant FTL1678 and FTT0101 were expressed and affinity purified from *E. coli*. As a control, lysates from *E. coli* containing the empty vector (pPROEX HTb) also were affinity-purified . Recombinant FTL1678, lysate from the vector control, or buffer alone were incubated with various PG precursors and PG intermediates (Table 1) to determine substrate specificity and specific activity. The vector control and buffer alone did not demonstrate activity against any of the PG substrates (data not shown). When FTL1678 was incubated with various PG substrates, the highest specific activity was detected against the tetrapeptide substrates GlcNAc-anhydroMurNAc-L-Ala-γ-D-Glu-*meso*-A_2pm-D-Ala (tracheal cytotoxin; TCT; 21.5 nmol/min/mg of protein) and GlcNAc-MurNAc-L-Ala-γ-D-Glu-*meso*-A_2pm-D-Ala (PG monomer; 15.6 nmol/min/mg of protein), confirming that FTL1678 exhibits L,D-carboxypeptidase activity (Table 1). Interestingly, FTL1678 activity against free tetrapeptide, L-Ala-γ-D-Glu-*meso*-A_2pm-D-Ala, was approx. 6-fold lower (3.4 nmol/min/mg of protein) than TCT and 5-fold lower than the PG monomer (Table 1), indicating that GlcNAc and MurNAc

may be important for tetrapeptide recognition or FTL1678 binding. Importantly, FTL1678 exhibited specific activity against pentapeptide substrates MurNAc-L-Ala-γ-D-Glu-*meso*-A_2pm-D-Ala-D-Ala (9.8 nmol/min/mg of protein; Table 1) and UDP-MurNAc-L-Ala-γ-D-Glu-*meso*-A_2pm-D-Ala-D-Ala (5.9 nmol/min/mg of protein; Table 1), indicating that FTL1678 also functions as an L,D-endopeptidase (cleavage of the pentapeptide between *meso*-A_2pm and D-Ala) by FTL1678.

FTL1678 had negligible activity against L-lysine-containing substrates (0.7 to 1.3 nmol/min/mg of protein; Table 1), where L-lysine replaced *meso*-A_2pm at the third amino acid position, indicating the importance of *meso*-A_2pm. Assays were repeated with recombinant FTT0101 (SchuS4 homolog), where FTT0101 demonstrated similar tetrapeptide cleavage activity (*i.e.*, LdcA activity) as FTL1678 (Table 1). FTT0101 also was not active on a peptidoglycan polymer and had either no or negligible activity on PG monomers that were amidated at the *meso*-A_2pm or D-Glu residues (Table 1). Additionally, FTT0101 was not inhibited by 5 mM EDTA and did not require the presence of cations (Mg^{2+}) for tetrapeptide cleavage (data not shown).

FTL1678 controls bacterial morphology

LdcA has been shown to be important for maintenance of bacterial morphology and structural integrity (32, 37). In addition, it is well-documented that mutation or deletion of other PG-modifying proteins results in abnormal bacterial morphology, emphasizing the importance of PG modification and recycling (13, 38-42). To assess if FTL1678 plays a similar role in *F. tularensis*, we generated an isogenic deletion of *FTL1678*, referred to hereafter as Δ*FTL1678*, in *F. tularensis* LVS. When examined by transmission electron microscopy (TEM), wild-type

(WT) bacterial width ranged from 350 to 800 nm (Fig. 3A and D), whereas Δ*FTL1678* were more uniform in cell width, averaging approx. 350 nm (Fig. 3B and D). WT bacteria were observed to be coccobacilli with loosely-associated OM (Fig. 3A), while Δ*FTL1678* were found to be coccoid and appeared to have a more tightly-associated OM (Fig. 3B). Additionally, Δ*FTL1678* bacteria appeared more electron dense and had a significantly-thicker OM than WT (Fig. 3A, B, and C).

Previous studies have shown that deletion of PG-modifying proteins (*e.g.,* murein hydrolases) can result in abnormal growth characteristics, including lysis during stationary phase (27) and an inability to separate daughter cells at the septa during cell division, resulting in abnormal bacterial chains (13, 15, 40, 41, 44-46). Although *N*-acetylmuramyl-L-alanine amidases have been shown to be predominantly involved in the cleavage of bacterial septa, deletion of lytic transglycosylases and some endopeptidases, in combination with amidase deletions, also have resulted in abnormal bacterial chains (41, 44). To examine if Δ*FTL1678* exhibited any of these septation defects or resulted in bacterial chains, we grew Δ*FTL1678* in supplemented Mueller Hinton Broth (sMHB; standard growth medium for *F. tularensis*; (34)), finding that it did not have an inherent growth defect (Fig. 4A). When examined by TEM, approximately 10% of Δ*FTL1678* bacteria grew in chains of three to four bacteria (Fig. S3), whereas no WT bacteria exhibited this septation defect. Considering that Δ*FTL1678* is 1.5- to 2-times smaller than WT (Fig. 3D), is more coccoid in shape (Fig. 3B), and has a partial septum defect (Fig. S3), these results further support the role of FTL1678 as a PG-modifying enzyme that is important for bacterial elongation and division.

Deletion of FTL1678 affects membrane integrity and permeability

To determine if there were differences in membrane integrity between WT and Δ*FTL1678*, we grew both bacteria in the presence of various antibiotics, detergents, and dyes, and measured zones of inhibition after 48 h of growth (Table 2). Δ*FTL1678* was more susceptible than WT to ampicillin, vancomycin, lysozyme, and SDS, indicating potential changes to PG, OM integrity, or efflux pumps. By comparison, Δ*FTL1678* was more resistant than WT to gentamicin, tetracycline, chloramphenicol, ciprofloxacin, ethidium bromide, and Triton X-100. Given that gentamicin, tetracycline, and chloramphenicol normally inhibit protein synthesis and ciprofloxacin and ethidium bromide normally interfere with DNA replication, these results indicate that Δ*FTL1678* has a less permeable envelope that prevents these inhibitory molecules from entering the cytoplasm. To better understand potential differences in Δ*FTL1678* PG, OM integrity, efflux pump activity, or envelope permeability, WT and Δ*FTL1678* were either grown in sMHB at 37°C or in various stress conditions. In sMHB, Δ*FTL1678* does not have an inherent growth defect but, instead, appeared to grow to a higher optical density (OD_{600}) than WT (Fig. 4A). However, bacterial enumeration at several time points revealed that there was no significant difference between WT and Δ*FTL1678* bacterial numbers at each time point (data not shown). Although speculative, differences in optical densities between WT and Δ*FTL1678* may be due to the morphological differences observed by TEM (Fig. 3 and S3). Compared with growth in sMHB, no substantial differences in the growth rates of WT and Δ*FTL1678* were observed at either 40°C or in the presence of 60 μM $CuCl_2$ (Fig. 4B and C). However, Δ*FTL1678* grew considerably better than WT in the presence of 5 mM H_2O_2, 5% NaCl, and pH 5.5 (Fig. 4D, E, and F), providing further evidence that Δ*FTL1678* has a less permeable envelope. These results also corroborate the increased OM thickness and more tightly associated OM in Δ*FTL1678*, compared to WT (Fig. 3).

FTL1678 and Ldc activity is required for *F. tularensis* virulence

To examine if FTL1678 plays a role in *F. tularensis* virulence, mice were intranasally infected with 10^4 CFU of either WT or Δ*FTL1678* and monitored daily for signs of disease. Whereas all WT-infected mice died by day 9 post-infection (median time-to-death day 6), Δ*FTL1678* was completely attenuated (100% survival through day 21 post-infection), demonstrating that FTL1678 is required for *F. tularensis* virulence (Fig. 5A). To confirm that the observed attenuation was solely due to the deletion of *FTL1678*, and not to polar effects, we complemented Δ*FTL1678* with a 6× His-tagged FTL1678 *in trans*, which fully-restored virulence to WT levels (all mice died by day 7; median time-to-death day 6; Fig. 5A).

To more carefully assess Δ*FTL1678* attenuation *in vivo*, we intranasally-infected mice with 10^4 CFU of either WT LVS or Δ*FTL1678*, and enumerated bacterial CFUs from lungs, livers, spleens, and blood on days 2 and 5 post-infection to examine bacterial replication and dissemination to these organs/tissues over time. On day 2 post-infection, WT LVS replicated to $>10^7$ CFU/mg lung and had disseminated to livers, spleens (approx. 10^3 CFU/mg), and blood (10^3 CFU/ml; Fig. 5B). In contrast, Δ*FTL1678* had an initial (day 2) colonization defect in the lungs (4-logs less than WT) and was unable to disseminate to livers, spleens, or blood (Fig. 5B). By day 5 post-infection, the attenuation of Δ*FTL1678* was even more apparent, with WT LVS replicating to extremely high numbers (approx. 10^8 CFU/mg) in lungs, livers, and spleens, compared with Δ*FTL1678*, which replicated approx. 1-log in lungs (between day 2 and 5), but was 4-log attenuated in lungs and was not detectable in livers or spleens. Although Δ*FTL1678* was detected in the blood on day 5, it was 2-logs less than WT LVS.

The Type A *F. tularensis* strain SchuS4 originally was isolated from a human tularemia patient and requires BSL3 containment. Given its relevance to human disease, we next generated an isogenic deletion mutant of the *FTL1678* homolog, *FTT0101*, in SchuS4. When mice were intranasally-infected with either WT SchuS4 or Δ*FTT0101*, all mice died by day 7 post-infection, indicating that *FTT0101* is not required for SchuS4 virulence (Fig. S4). Whereas Δ*FTT0101*-infected mice exhibited a slightly delayed time-to-death (median time-to-death day 6; Fig. S4), compared with WT SchuS4-infected mice (median time-to-death day 5; Fig. S4), this may be due to differences in the infectious dose administered to mice in this experiment (80 CFU SchuS4; 12 CFU Δ*FTT0101*). However, it also remains possible that the extreme virulence of SchuS4 (intranasal LD_{50} <10 CFU in our hands) complicates assessments of mutant attenuation.

FTL1678 and Ldc activity, but not the LdcA catalytic triad, are required for *F. tularensis* virulence

As noted above and highlighted in Fig. 1, *P. aeruginosa* LdcA contains a Ser-His-Glu catalytic triad which is essential for function and is characteristic of Ldc in the Peptidase_S66 family (30). The Ser-His-Glu catalytic triad also has been confirmed in Ldc from *E. coli* (47), *Novosphingobium aromaticivorans* (48), and *N. gonorrhoeae* (31). Given the relatively conserved spacing of Ser-His-Glu residues in FTL1678 (Fig. 1), we tested if these residues were required for *F. tularensis* virulence (similar to Fig. 5A virulence assessments for Δ*FTL1678* and the FTL1678 complemented strain). Site-directed mutagenesis was performed to independently generate FTL1678 complementation constructs containing either S134A, H308A, or E239A mutations. Next, Δ*FTL1678* was complemented *in-trans* with each of these FTL1678 catalytic triad point mutants, and mice were intranasally infected with either WT, Δ*FTL1678*, FTL1678

trans-complement, or one of the FTL1678 catalytic triad point mutant *trans*-complements (referred to hereafter as S134A, H308A, and E239A). Whereas Δ*FTL1678* was completely attenuated (100% survival through day 21), complementation of Δ*FTL1678* with either FTL1678 (all mice dead by day 8), S134A (all mice dead by day 7), H308A (all mice dead by day 8), or E239A (all mice dead by day 8), fully-restored virulence to WT LVS levels (all mice dead by day 10; Fig. S5), indicating that although a putative Ser-His-Glu catalytic triad is present in FTL1678, these residues are not individually important for *F. tularensis* virulence.

The Ldc ortholog alignment (Fig. 1) also highlighted that, of the six Ldc orthologs examined here, only *C. jejuni* Pgp2 lacked the Ser-His-Glu catalytic triad. However, *C. jejuni* Pgp2 previously was shown to exhibit LdcA activity (32), indicating that a Ser-His-Glu catalytic triad is not required for LdcA function. To further assess if LdcA activity, independent of a Ser-His-Glu catalytic triad, was required for *F. tularensis* virulence, we complemented Δ*FTL1678* with a 6× His-tagged Pgp2 from *C. jejuni* and infected mice with either WT LVS, Δ*FTL1678*, Δ*FTL1678 trans*-complemented with FTL1678, or Δ*FTL1678 trans*-complemented with *C. jejuni* Pgp2. While Δ*FTL1678* was fully attenuated (100% survival through day 21), the Pgp2 *trans*-complement was fully-virulent (median time-to-death 6 days; all mice dead by day 7), nearly identical to WT LVS (median time-to-death 7 days; all mice dead by day 7) and the FTL1678 *trans*-complement (median time-to-death 6 days; all mice dead by day7; Fig. 5C), providing further evidence that FTL1678 is an Ldc and Ldc activity is required for *F. tularensis* virulence.

To provide additional evidence that FTL1678 exhibits Ldc activity and that *C. jejuni* Pgp2 functionally complements Δ*FTL1678*, the FTL1678 *trans*-complement and Pgp2 *trans*-complement were examined by TEM, revealing that both complemented strains had similar

morphology as WT LVS (Fig. S6A and B; Fig. 3A). Additionally, OM thickness and cell width were measured for WT, Δ*FTL1678*, and both complemented strains, demonstrating that both complemented strains had OM thicknesses and cell widths similar to WT, and both complemented strains were significantly different from Δ*FTL1678* (Fig. S6C and D). Finally, when grown in the presence of various stressors (*e.g.*, 5 mM H_2O_2, 5% NaCl, pH 5.5, antibiotics, SDS, lysozyme, or ethidium bromide), both complemented strains exhibited similar phenotypes as WT LVS (Fig. S6E, F, G, and H and Table S4).

FTL1678 is required for *F. tularensis* replication in macrophages

F. tularensis is an intracellular pathogen and macrophages appear to be one of the major targets for *F. tularensis* infection and replication (49-51). To investigate potential replication defects of Δ*FTL1678* in macrophages, J774A.1 macrophages or murine bone marrow-derived macrophages (mBMDM) were infected with either WT LVS or Δ*FTL1678* (MOI 100:1) and bacterial numbers were enumerated at 0 h (entry), 6 h, and 24 h post-infection. At entry (0 h), approx. 2.5-logs more Δ*FTL1678* were present in both macrophage lines, compared with WT LVS (Fig. 6A). This likely was due to the above noted gentamicin resistance of Δ*FTL1678* (Table 2). Attempts to normalize entry numbers for both WT LVS and Δ*FTL1678*, using different antibiotics or combinations of antibiotics, were not successful. Despite higher numbers of Δ*FTL1678* in both macrophages at entry and 6 h, Δ*FTL1678* was unable to replicate in either macrophage, and decreased approx. 1-log from 6 h to 24 h (Fig. 6A). By comparison, WT LVS numbers increased 1.5- to 2-logs from 6 h to 24 h (Fig. 6A). To normalize WT LVS and Δ*FTL1678* bacterial numbers or replication rates in both macrophages, fold change in bacterial numbers was calculated from 6 h to 24 h: WT was found to increase 2.5- and 1.5-logs in J774A.1

cells and mBMDMs, respectively, whereas Δ*FTL1678* was found to decrease 0.5- to 1-log, respectively (Fig. 6B). Taken together, these *in vitro* results (Fig. 6A and B) confirm the observed *in vivo* attenuation of Δ*FTL1678* (Fig. 5A and B).

Δ*FTL1678* protects mice against Type A *F. tularensis* infection

No FDA-approved vaccine currently is available to prevent tularemia. In addition, *F. tularensis* is designated as an NIH category A priority pathogen and CDC Tier 1 Select Agent, highlighting the extreme virulence of this bacterium and the need for a safe and effective vaccine to prevent tularemia. Given our above findings that 10^5 CFU of Δ*FTL1678* did not cause disease or death in mice (Fig. 5A), we next examined whether high doses (10^7 or 10^9 CFU) of Δ*FTL1678* were attenuated or if Δ*FTL1678* immunization could protect mice from fully-virulent Type A *F. tularensis* SchuS4 challenge. First, all mice intranasally immunized with either 10^5, 10^7, or 10^9 CFU of Δ*FTL1678* survived through day 28 post-infection, with no signs of clinical disease (Fig. 7A). Second, on day 29, all mice were boosted with 10^9 CFU of Δ*FTL1678* and no mice demonstrated any signs of disease through day 50 (Fig. 7A). Third, on day 51, mice were intranasally-challenged with 120 CFU (6× the LD_{50}) of SchuS4 and the health status of each immunization group was monitored for an additional 26 days. In a dose-dependent manner, the 10^9 prime-10^9 boost regimen conferred 80% protection, the 10^7 prime-10^9 boost regimen conferred 40% protection, and the 10^5 prime-10^9 boost regimen conferred 20% protection (Fig. 7B). These data demonstrate that Δ*FTL1678* is highly attenuated (up to 10^9 CFU) and that Δ*FTL1678* may be able to be used as a live, attenuated vaccine.

Δ*FTL1678* does not cause tissue damage

The *in vitro* (Fig. 6) and *in vivo* (Fig. 5A, 5B, 7A) attenuation of Δ*FTL1678*, as well as protection against SchuS4 pulmonary challenge (Fig. 7), indicated that Δ*FTL1678* could be used as a live, attenuated vaccine. While live, attenuated vaccines have been extremely effective at preventing a number of diseases, they can pose safety challenges (52, 53). To assess whether Δ*FTL1678* immunization induced any pathology in immunized mice, lungs, livers, and spleens from uninfected, WT LVS-, or Δ*FTL1678*-infected mice were assessed for pathologic changes on day 5 post-infection/immunization. WT LVS-infected lungs demonstrated alveolar wall thickening, large areas of inflammation, and severe neutrophil infiltration (Fig. 8A). By comparison, little inflammation was observed in Δ*FTL1678*-infected lungs, although some red blood cell congestion was present, indicating a limited, acute immune response that was quickly resolved (Fig. 8A). Whereas WT LVS-infected livers were characterized by diffuse inflammation with focal areas of necrosis, Δ*FTL1678*-infected livers were virtually indistinguishable from uninfected livers, with no observable pathology (Fig. 8A). Finally, although the architecture of WT LVS-infected spleens lacked distinct areas of white pulp or red pulp, indicative of a severe infection, Δ*FTL1678*-infected spleens were observed to contain distinct areas of red pulp and white pulp, with some red blood cell congestion – indicating a limited, acute immune response that was quickly resolved (Fig. 8A). All tissues were blindly scored using a pathology severity index (scale from 0 to 4, with 4 indicating severe pathology), confirming that Δ*FTL1678*-infected tissues were virtually indistinguishable from uninfected tissues (pathology scores of 1 for lungs, 0 for liver, and 1.5 for spleens) and WT LVS-infected tissues had significantly higher pathology scores (pathology scores >3.5 for all tissues; Fig. 8B).

Discussion

Bacterial PG is a complex, mesh-like structure, composed of a glycan backbone, crosslinked to varying degrees, by peptide chains (54). It is well known that this structure plays an important role in maintaining Gram-negative bacterial cell morphology, membrane integrity, regulating changes in osmotic pressure, and providing a platform for attachment of the OM (55, 56). Although a majority of PG studies have focused on how the thick layer of PG in Gram-positive bacteria contributes to virulence and antibiotic resistance, more recent studies have highlighted that Gram-negative PG also is intimately linked with pathogenicity (13).

PG recycling is an essential function of Gram-negative bacteria during cell growth and division to produce new cell wall components. In fact, Gram-negative bacteria recycle up to 50% of their PG with every generation, suggesting that both PG synthesis and PG recycling are dynamic (1, 10). A number of proteins are involved in these processes and, while they are well-characterized in *E. coli*, very little is known about these pathways in intracellular pathogens such as *Burkholderia pseudomallei*, *Legionella pneumophila*, or *F. tularensis* (57-60).

E. coli LdcA, a cytoplasmic protein, was the first L,D-carboxypeptidase to be identified and was shown to be important for PG recycling and survival during stationary phase (27, 29). More recently, Ldcs have been identified in *P. aeruginosa* (30), *C. jejuni* (32), *N. gonorrhoeae* (61), and *N. aromaticivorans* (48). In this study, we identified an *F. tularensis* PG recycling enzyme, FTL1678, which we propose naming LdcA. Unlike well-characterized cytoplasmic LdcAs from *E. coli* and *P. aeruginosa*, we demonstrated that *F. tularensis* LdcA was localized to OM fractions and, given co-localization with PG-associated proteins Pal and TolB, is most likely located on the inner leaflet of the OM or in the periplasm. At this time, we can only speculate on why most Gram-negative bacteria encode cytosolic LdcAs but *F. tularensis* encodes a periplasmic LdcA, but in the context of PG repair and recycling, periplasmic LdcA certainly

offers a fitness advantage. This is not the first report of a periplasmic LdcA, as *C. jejuni* Pgp2 is predicted to be periplasmic and *N. gonorrhoeae* LdcA is periplasmic (31, 32).

Our results demonstrated, for the first time, that *F. tularensis* LdcA directly acts on the tetrapeptides TCT and PG monomer. More importantly, we also found that *F. tularensis* LdcA directly cleaves the pentapeptide to a tripeptide, highlighting that *F. tularensis* LdcA is a multi-functional enzyme that performs both L,D-carboxypeptidase and L,D-endopeptidase activities (Table 1). In addition, we demonstrated that *F. tularensis* LdcA cleaves PG pentapeptides without a prior cleavage event by a D,D-carboxypeptidase/Penicillin Binding Protein (PBP), such as DacD. It should be noted that although *N. gonorrhoeae* LdcA has been reported to have L,D-endopeptidase activity, this activity is specific to tetrapeptide cross links (4-3 and 3-3 links) (31). Interestingly, only two previous studies have examined putative *F. tularensis* PG modifying enzymes. In both studies, the authors primarily focused on the role of a *F. tularensis* DacD ortholog in virulence, with no PG activity assays to confirm function (59, 60). In our PG cleavage analysis, *F. tularensis* LdcA demonstrated the highest specific activity on disaccharide-tetrapeptide PG substrates (GlcNAc-anhydroMurNAc-L-Ala-γ-D-Glu-*meso*-A_2pm-D-Ala [TCT] and GlcNAc-MurNAc-L-Ala-γ-D-Glu-*meso*-A_2pm-D-Ala [PG monomer]), followed by cleavage of pentapeptide PG substrates (MurNAc-L-Ala-γ-D-Glu-*meso*-A_2pm-D-Ala-D-Ala and UDP-MurNAc-L-Ala-γ-D-Glu-*meso*-A_2pm-D-Ala-D-Ala). Despite high specific activity of *F. tularensis* LdcA on tetrapeptide attached to the disaccharide, *F. tularensis* LdcA demonstrated approximately 6-times lower specific activity on free tetrapeptide (no sugars) (Table 1). In contrast, *E. coli* LdcA has been shown to have the highest specific activity on free tetrapeptide, monosaccharide-tetrapeptide (MurNAc-L-Ala-γ-D-Glu-*meso*-A_2pm-D-Ala), and monosaccharide tetrapeptide linked to a glycan lipid carrier (UDP-MurNAc-tetrapeptide) (27),

but is unable to cleave dimeric muropeptides. Additionally, *F. tularensis* LdcA was active against the TCT dimer (two crosslinked TCT monomers), but not PG polymers. Although purely speculative, this TCT dimer cleavage potentially indicates that *F. tularensis* LdcA may possess endopeptidase activity on peptide cross-links.

Previous studies have shown that Ldcs are important for cell morphology and membrane integrity. Deletion of the Ldc homologs Csd6 from *H. pylori* (37) and Pgp2 from *C. jejuni* (32) resulted in loss of helical morphology. Here, we demonstrated that FTL1678 is essential for maintaining the coccobacillus morphology of *F. tularensis*, as Δ*FTL1678* were significantly-smaller cocci that were more electron dense than WT. Δ*FTL1678* had significantly thicker envelopes than WT bacteria and the Δ*FTL1678* OM was more tightly-associated with the bacteria, compared to WT OMs that appeared to be loosely-associated. It is possible that deletion of *FTL1678* may have prevented efficient recycling or breakdown of existing PG, resulting in a buildup of pentapeptides or tetrapeptides that are highly-crosslinked. However, repeated attempts to isolate and analyze *F. tularensis* PG have been unsuccessful and, therefore, we can only speculate on the true nature of the thick envelope in Δ*FTL1678*.

Due to the increased thickness of the envelope and altered cell morphology of Δ*FTL1678* observed by TEM, we investigated differences in membrane integrity between WT and Δ*FTL1678*, finding that Δ*FTL1678* was more susceptible to several compounds including ampicillin, vancomycin, lysozyme, and SDS. Vancomycin, usually not effective against Gram-negatives due to its inability to penetrate the OM, inhibited Δ*FTL1678* growth, indicating increased permeability of the Δ*FTL1678* OM. Vancomycin may have been especially effective on Δ*FTL1678* because its mechanism of action includes binding to the two terminal D-Ala-D-Ala residues of PG pentapeptide chains and preventing cross-linking of monomers. Δ*FTL1678*

also may have increased the amount of pentapeptides present in PG, providing more targets for vancomycin action.

We also found that Δ*FTL1678* was more resistant to several stressors, including gentamicin, tetracycline, chloramphenicol, ciprofloxacin, ethidium bromide, Triton-X 100, H_2O_2, pH 5.5, and high NaCl. Although the specific mechanism for increased resistance of Δ*FTL1678* to these compounds is unclear, we hypothesize that the thick PG of Δ*FTL1678* may be more highly crosslinked, preventing large compounds like gentamicin, tetracycline, chloramphenicol, ciprofloxacin, ethidium bromide, and Triton-X 100 from getting through and/or may have increased the expression of efflux pumps to efficiently remove toxic compounds from the bacteria.

Due to the extreme virulence of Type A *F. tularensis* and its designation as a Tier 1 Select Agent, identification of virulence factors and development of new vaccines is important. In this study, we identified the role of a previously unstudied protein, FTL1678, in PG recycling and envelope integrity maintenance, we demonstrated that FTL1678 was required for *F. tularensis* LVS virulence, and we found that Δ*FTL1678* conferred 80% protection against fully-virulent, Type A *F. tularensis* SchuS4 pulmonary challenge. Further studies are needed to determine specific immune responses induced by Δ*FTL1678* immunization, as well as identify the most effective immunization regimen (*e.g.*, number of immunizations and time between immunizations).

Finally, given the importance of PG in *F. tularensis* virulence, we used bioinformatic approaches to predict the proteins involved in *F. tularensis* PG synthesis and recycling (Fig. 9). With the exception of DacD, none of the predicted PG-associated proteins previously have been studied and homologues could not be found for at least seven genes/proteins (Fig. 9). Given our

observed attenuation of Δ*FTL1678*, the PG synthesis and recycling pathways may offer more opportunities to better understand the virulence of *F. tularensis* and other intracellular pathogens. Characterization of other proteins involved in PG pathways may provide clues as to why *F. tularensis* LdcA is periplasmic and encodes both L,D-carboxypeptidase and L,D-endopeptidase activities.

Materials and Methods

Bacterial strains and culture conditions. *F. tularensis* Type A strain SchuS4 and *F. tularensis* Type B strain LVS were obtained from BEI Resources and cultured as previously described (24, 43). All experiments with SchuS4 were performed under BSL3 containment conditions at the University of Toledo Health Science Campus BSL3 laboratory. Routine *F. tularensis* cultures were grown overnight at 37°C with 5% CO_2 on supplemented Mueller-Hinton agar (sMHA): Mueller-Hinton broth powder (Becton Dickinson) was mixed with 1.6% (wt/vol) Bacto Agar (Becton Dickinson), autoclaved, and further supplemented with 2.5% (vol/vol) bovine calf serum (Hyclone), 2% (vol/vol) IsoVitaleX (Becton Dickinson), 0.1% (wt/vol) glucose, and 0.025% (wt/ vol) iron pyrophosphate. For mouse infections, *F. tularensis* was first grown on sMHA then transferred to Brain Heart Infusion agar (BHI; Becton Dickinson). Chocolate agar for mutant strain generation was prepared by mixing Mueller Hinton broth powder with 1.6% (wt/vol) agar, 1% (wt/vol) tryptone, and 0.5% (wt/vol) sodium chloride, autoclaved, and further supplemented with 1% (wt/vol) hemoglobin and 1% (vol/vol) IsoVitaleX. For macrophage infections, *F. tularensis* was first grown on sMHA then transferred

to modified chocolate agar: Mueller-Hinton broth powder was mixed with 1.6% (wt/vol) Bacto Agar, 1% hemoglobin (wt/vol), and 1% (vol/vol) IsoVitaleX. All growth curves were performed in sMHB: Mueller-Hinton broth powder was mixed with 182 mg/L calcium chloride dihydrate, and 210 mg/L magnesium chloride hexahydrate, 0.1% (wt/vol) glucose, 0.025% (wt/vol) iron pyrophosphate, and 2% (vol/vol) IsoVitaleX. All bacterial strains and plasmids are listed in Table S1. *Escherichia coli* S17-1 and *E. coli* NEB10-β were grown in Luria Bertani (LB) broth or on LB agar at 37°C, supplemented as needed with antibiotics.

Sequence Alignments and Bioinformatic Predictions. Amino acid alignments of *F. tularensis* subsp. *holarctica* FTL_1678, *F. tularensis* subsp. *tularensis* FTT_0101, *E. coli* LdcA (BAA36050.1), *P. aeruginosa* LdcA (Q9HTZ1), *N. gonorrhoeae* (YP_208343.1), and *C. jejuni* Pgp2 (WP_002856863) were performed using Clustal Omega (https://www.ebi.ac.uk/Tools/msa/clustalo/) and MView (https://www.ebi.ac.uk/Tools/msa/mview/). Pairwise sequence alignments were performed and amino acid identities among Ldc homologues were calculated by EMBOSS Needle (https://www.ebi.ac.uk/Tools/psa/emboss_needle/). The Prokaryotic Genome Analysis Tool (PGAT) (http://tools.uwgenomics.org/pgat/), BlastP, and BlastX analyses (http://blast.ncbi.nlm.nih.gov) were used to identify *F. tularensis* homologues. Bacterial protein sub-localization was predicted by PSORTb version 3.0.2 (https://www.psort.org/psortb/). Protein signal sequence prediction was performed by LipoP version 1.0 (http://www.cbs.dtu.dk/services/LipoP/) and SignalP version 4.1 (http://www.cbs.dtu.dk/services/SignalP-4.1/).

Generation of *F. tularensis* gene deletion mutants. *F. tularensis* isogenic deletion mutants were generated by homologous recombination as previously described (62). Briefly, 500 bp regions upstream and downstream from the gene of interest (*FTL1678* or *FTT0101*) were PCR-amplified from *F. tularensis* genomic DNA using the following primers: FTL1678_A and FTL1678_B; FTL1678_C and FTL1678_D; FTT0101_A and FTT0101_B; FTT0101_C and FTT0101_D (Table S2). A FLP recombination target (FRT)-flanked Pfn-kanamycin resistance cassette, FRT-Pfn-kan-FRT, was PCR amplified from pLG66a (63) and splicing overlap extension PCR (SOE PCR) was used to join the upstream (A-B) and downstream (C-D) regions with FRT-Pfn-kan-FRT, which replaced the gene of interest. The resulting insert and a suicide plasmid, pTP163 (64), were digested with ApaI (New England Biolabs), and ligated using T4 DNA ligase (New England Biolabs). Gene deletion constructs were transformed into NEB10-β *E. coli* (New England Biolabs), sequence-verified, transformed into *E. coli* S17-1, and conjugation was performed with *F. tularensis* LVS on sMHA plates. Conjugants were recovered on chocolate agar supplemented with 200 mg/L hygromycin and 100 mg/L polymyxin B. Individual mutants were selected by sequential plating on sMHA supplemented with 10 mg/L kanamycin (sMHA-kan10), sMHA-kan10 with 8% (wt/vol) sucrose, and final replica plating onto sMHA containing either 200 mg/L hygromycin (sMHA-hyg200) or sMHA-kan10. Hyg-sensitive and kan-resistant colonies were sequence verified (referred to hereafter as either Δ*FTL1678* or Δ*FTT0101*).

***FTL1678* complementation *in trans*.** Complementation *in trans* was performed as previously described, with some modifications (43). *FTL1678* was PCR-amplified from *F. tularensis* LVS using primers 5'FTL1678_NEBuilder and 3'FTL1678_NEBuilder (Table S2),

pQE-60 (Qiagen) was double-digested with NcoI and BglII (New England Biolabs), and the NEBuilder HiFi DNA Assembly Cloning kit was used to ligate the *FTL1678* amplicon and digested pQE-60. The construct was transformed into NEB 10-β *E. coli* and transformants were selected on LB agar supplemented with 100 mg/L ampicillin (LB-amp). Plasmids were purified from individual clones using the Qiagen QIAprep Spin Miniprep kit (Qiagen), diagnostic PCR was performed to confirm insert presence and correct size, and DNA sequencing was performed to verify insert integrity. The resulting construct, *FTL1678* with a C-terminal 6x histidine tag, was PCR-amplified using primers 5'FTL1678_pFNLTP6 and 3'FTL1678_pFNLTP6 (Table S2), the amplicon and pFNLTP6-gro-GFP (65) were double-digested with XhoI and BamHI (New England Biolabs), and ligated using T4 DNA Ligase. The construct, pFNLTP6-gro-*FTL1678*-6xHis, was transformed into NEB10-β *E. coli*, transformants were selected on LB plates supplemented with 50 mg/L kanamycin (LB-kan), and DNA sequencing was performed to verify FTL1678-6xHis integrity. Next, the kan resistance gene was removed from Δ*FTL1678* by suspending the strain in 0.5 M sucrose (in 1 mM EDTA, pH 7.5), washing three times, and electroporating the shuttle plasmid pTP405 (64), which encodes the Flp recombinase to remove FRT-Pfn-kan-FRT from the genome. Bacteria were grown overnight on sMHA-hyg200, hyg-resistant transformants were passaged three times on sMHA, then transformants were replica plated onto sMHA-hyg200 and sMHA-kan10 to confirm sensitivity to both antibiotics (kan-cured Δ*FTL1678*). pFNLTP6-gro-*FTL1678*-6xHis was transformed into kan-cured Δ*FTL1678* by electroporation, transformants were selected on sMHA-kan10, and expression of FTL1678 was confirmed by immunoblot analysis (referred to hereafter as Δ*FTL1678 trans*-complement).

C. jejuni* Pgp2 complementation *in trans. Complementation of *C. jejuni pgp2* (CJJ81176_0915) into Δ*FTL1678* was performed as described above, with several modifications. The *pgp2* gene, with the FTL1678 signal sequence (amino acid residues 1-29) in place of the native Pgp2 signal sequence (amino acid residues 1-18), was synthesized and inserted in pQE-60 by GenScript USA. pQE-60-*pgp2* was transformed into NEB10-β *E. coli* and selection was performed on LB-amp. Pgp2-6xHis was amplified from pQE-60 using primers 5'FTL1678_pFNLTP6 and 3'FTL1678_pFNLTP6 (Table S2), the amplicon was ligated into similarly digested pFNLTP6, pFNLTP6-gro-*pgp2*-6xHis was transformed into NEB10-β *E. coli*, and transformants were selected on LB-kan. Plasmids were purified from kan-resistant transformants, sequence verified, then electroporated into kan-cured Δ*FTL1678*. Pgp2 expression was confirmed by immunoblot analysis.

Mouse Infections. All animal studies were approved by the University of Toledo Institutional Animal Care and Use Committee (IACUC). Mouse infections were performed as previously described (66), with some modifications. Briefly, *F. tularensis* strains were grown on sMHA overnight, transferred to BHI agar for an additional 20-24 h, suspended in sterile PBS, and diluted to the desired concentration (20 to 10^9 CFU/20 µl) based on previous OD_{600} measurements and bacterial enumeration studies. Groups of 4-8 female C3H/HeN mice (6-8 weeks old; Charles River Laboratories) were anesthetized with a ketamine-xylazine sedative and intranasally (i.n.) infected with 20 µl of prepared bacterial suspensions. Bacterial innocula were serially-diluted and plated in quadruplet on sMHA to confirm CFUs. For survival studies, mice were monitored daily, for signs of disease, with health status scores (scale of 1-5, with 1 indicating healthy and 5 indicating mouse found dead) being recorded for each mouse.

Moribund mice were humanely euthanized to minimize suffering. To quantitate bacterial tissue burdens, groups of 4 mice were euthanized on days 2 and 5 post-infection, blood was collected by cardiac puncture and plated onto sMHA, lungs, livers, and spleens were aseptically harvested, homogenized, 25 µl of PBS/mg of tissue was added to each tissue, serially-diluted, and dilutions were plated onto sMHA. Following 72 h of incubation, the number of colonies per plate were counted and CFU/mg (tissues) or CFU/ml (blood) were calculated based on tissue weight and dilution factor. For immunization and challenge studies, groups of 4-10 mice were i.n. immunized with either 100-300 CFU LVS or 10^4-10^9 CFU ΔFTL1678, boosted 3-4 weeks later with either 10^3 CFU LVS or 10^9 CFU ΔFTL1678, transported to the ABSL3 facility 3-weeks later, and i.n. challenged with 20-120 CFU of *F. tularensis* SchuS4. Mice were monitored daily for signs of disease with health status scores being recorded for each mouse.

Membrane Integrity Testing. Sensitivity of LVS, Δ*FTL1678*, FTL1678 *trans*-complement, and the Pgp2 *trans*-complement to various antibiotics, detergents, dyes, and cell wall stressors was determined by disk diffusion assays or in liquid cultures, as previously described (43), with some modifications. Bacterial strains were grown on either sMHA or sMHA-kan10 (ΔFTL1678 and complement strains), scraped and resuspended in sterile PBS, adjusted to an OD_{600} of 0.2 (approx. $9x10^7$ CFU/ml), diluted 1:1 in PBS, and 100 µl was plated onto sMHA plates using cotton tipped applicators (Puritan). Sterile paper disks (Whatman; 0.8 mm thick, 6.5 mm in diameter) were placed in the center of each plate and antibiotics, detergents, or dyes were added to the disks at the concentrations listed in Table 2. Antibiotics tested were: gentamicin (Gibco), tetracycline (Fisher Scientific), chloramphenicol (Acros Organics), ciprofloxacin (Oxoid), ampicillin (Fisher Scientific), vancomycin (Acros Organics),

bacitracin (Oxoid), bacitracin (Oxoid), ciprofloxacin (Oxoid), and polymyxin b (MP Biomedicals). Detergents tested were: sodium dodecyl sulfate (SDS; anionic; Fisher Scientific), Triton X-100 (nonionic; Acros Organics), cetyltrimethyl ammonium bromide (CTAB; cationic; MP Biomedicals), 3-cholamidopropyl dimethylammonio 1-propanesulfonate (CHAPS; zwitterionic; Thermo Scientific). In addition, sensitivity to ethidium bromide (Thermo Scientific) and lysozyme (Thermo Fisher) also was tested. After 48 h, diameters of zones of inhibition around the disks were measured. Experiments were performed in triplicate. For liquid cultures, bacteria were suspended in sMHB, adjusted to OD_{600} 0.4, and 5 ml of each bacterial suspensions was inoculated into 100 ml of either sMHB or sMHB with 5 mM hydrogen peroxide (H_2O_2), 5% sodium chloride (NaCl), or pH 5.5 (pH of sMHB is 6.5). Cultures were grown at 37˚C with rotation at 180 rpm for 24 h with OD_{600} readings recorded every 4 hours.

Electron Microscopy. Electron microscopy was used to visualize differences in bacterial envelope structure and cell shape, as previously described (43), with some modifications. LVS, Δ*FTL1678*, FTL1678 *trans*-complement, and the Pgp2 *trans*-complement were grown overnight in sMHB, approx. $1x10^9$ CFU of each bacterial strain was pelleted by centrifugation at 7000 × *g* at 4˚C, washed three times in PBS, fixed in 3% (vol/vol) glutaraldehyde (Electron Microscopy Sciences [EMS]) for approx. 24 hours, washed twice in sodium cacodylate buffer (pH 7.4; EMS) for 10 min, suspended in 1% (wt/vol) osmium tetroxide (EMS) in s-collidine buffer (pH 7.4; EMS) for 45 min at room temperature (r/t) to stain and fix the samples, washed two times with sodium cacodylate buffer for 10 min each, and tertiary fixation was performed using an aqueous saturated solution of uranyl acetate (pH 3.3; EMS) for 45 min at r/t. Samples were then dehydrated at room temperature using a series of

ethanol washes: two washes with 30% ethanol for 10 min each; two washes with 50% ethanol for 10 min each; two washes with 95% ethanol for 10 min each; two washes with 100% ethanol for 10 min each; and two washes with 100% acetone for 10 min each. Samples were then infiltrated with 50% acetone and 50% embedding media (Hard Plus Resin 812, EMS) for 8 h to overnight at r/t. Samples were embedded in 100% embedding media (EMS) and allowed to polymerize for 8 h to overnight at 85°C, then sectioned at 85–90 nm, and visualized using a Tecnai G2 Spirit transmission electron microscope (FEI) at 80 kV and Radius 1.3 (Olympus) camera software at the University of Toledo Electron Microscopy Facility.

Spheroplasting and Sucrose Density Gradient Centrifugation. Spheroplasting, osmotic lysis, and sucrose density gradient centrifugation was performed as previously described (34) to determine subcellular localization of FTL1678. Briefly, the histidine-tagged FTL1678 *trans*-complement was grown in sMHB to an OD_{600} of 0.3-0.4, pelleted at 7500 × *g* for 30 min at 10˚C, supernatants were removed, pellets were resuspended in 0.75 M sucrose (in 5 mM Tris, pH 7.5) with gentle mixing, 10 mM EDTA (in 5 mM Tris, pH 7.8) was slowly added over 10 min, and the suspension was incubated for 30 min at r/t. After incubation, lysozyme was slowly added to a final concentration of 200 μg/ml, incubated for 30 min at r/t, bacteria were osmotically lysed by dilution into 4.5 × volume of molecular-grade water (Corning) over 11 min with gentle mixing, and incubated for 30 min at r/t. Lysates were centrifuged at 7,500 × *g* for 30 min at 10°C to remove intact cells and cellular debris. Supernatants were collected and centrifuged at 182,500 × *g* for 2 h at 4°C in a F37L 8 × 100 Fiberlite Ultracentrifuge rotor. Following centrifugation, supernatants were removed, membrane pellets were gently resuspended in 6 ml of resuspension buffer (25% [wt/wt] sucrose, 5 mM Tris, 30 mM $MgCl_2$, 1

tablet of Pierce Protease Inhibitor Mini Tablets, EDTA-Free [Thermo Scientific], 5 U Benzonase [Novagen]), suspensions were incubated with gentle mixing for 30 min at room temperature to degrade DNA, and a DC protein assay (Bio-Rad) was performed to determine total protein yield. Linear sucrose gradients were prepared by layering 1.8 ml each of sucrose solutions (wt/wt; prepared in 5 mM EDTA, pH 7.5) into 14- by 95-mm ultracentrifuge tubes (Beckman) in the following order: 55%, 50%, 45%, 40%, 35%, and 30%. Membrane suspensions were layered on top of each sucrose gradient, with less than 1.5 mg of protein per gradient. Sucrose gradients were centrifuged in an SW40 swinging bucket rotor (Beckman) at 256,000 × *g* for 17 h at 4°C. After centrifugation, 500 µl fractions were collected from each gradient by puncturing the bottom of each tube and allowing fractions to drip into microcentrifuge tubes. The refractive index of each fraction was determined using a refractometer (Fisher Scientific) and correlated with a specific density in g/ml (67) to identify outer membrane (OM; 1.17-1.20 g/ml) and inner membrane (IM; 1.13-1.14 g/ml) fractions. Sucrose gradient fractions were examined by immunoblotting as described below.

Immunoblotting. Whole cell lysates of FTL1678 *trans*-complement were prepared by suspending bacteria (pelleted at 7000 × *g*) in molecular biology grade water, diluting with SDS-PAGE loading buffer, and boiling for 10 min. Whole cell lysates, OM fractions, IM fractions, and molecular mass standards (Precision Plus protein all blue prestained protein standards; BioRad Laboratories) were separated on a 12.5% polyacrylamide gel, transferred to nitrocellulose, and blots were incubated overnight in blot block (0.1% (vol/vol) Tween 20 and 2% (wt/vol) bovine serum albumin in PBS) at 4°C. Immunoblotting was performed using rat

polyclonal antiserum specific for either *F. tularensis* OM protein FopA, *F. tularensis* IM protein SecY (34) or the Penta-His HRP conjugate antibody (Qiagen).

Infections of Mouse Bone Marrow Derived Macrophages (mBMDMs) and J774A.1 cells. Macrophage culture (37˚C with 5% CO_2 unless otherwise indicated) and infections were performed as previously described (43), with some modifications. Bone marrow macrophages were harvested from female C3H/HeN mice. Mice were euthanized by CO_2 asphyxiation and cervical dislocation. Femurs and tibias of both hind legs were aseptically-harvested, marrow was flushed from each bone with RPMI-1640 (Hyclone) containing 10% heat-inactivated fetal bovine serum ([HI-FBS], Atlanta Biologicals) and 30% supernatants from day 7 L929 cultures (ATCC). Bone marrow was disrupted by repeated passage through a 23-gauge needle and cultured for 4 days. Next, cell media was removed and replaced with RPMI containing 10% HI-FBS and 30% supernatant from day 14 L929 cultures, and cells were cultured for 2 days. Approx. 24 h before infection, media was removed, cells were harvested by scraping and centrifugation at 400 × *g* for 10 min at 10˚C, cells were enumerated using a hemocytometer, and diluted to $1x10^5$ cells in RPMI containing 10% HI-FBS. J774A.1 cells (ATCC) were cultured in Dulbecco's Modified Eagle Medium ([DMEM], Gibco) containing 10% HI-FBS. Approx. 24 h before infection, cells were harvested as described above, seeded into individual wells of 24-well plates (Corning) at a concentration of $1x10^5$ cells/well, and incubated overnight. mBMDMs and J774A.1 cells were infected with a multiplicity of infection (MOI) of 100 bacteria to 1 cell (100:1). Following infection, cells were centrifuged at 1,000 × *g* for 10 min at 4˚C, incubated at 37˚C with 5% CO_2 for 1 h, washed 1 × with RPMI (or DMEM), media containing 100 µg/ml gentamicin was added to kill extracellular bacteria, cells were incubated at 37˚C with 5% CO_2 for 1 h, washed 1x with

RPMI (or DMEM), lysed with 1% saponin for 4 min, serially diluted in PBS, plated onto sMHA plates, and bacteria were enumerated (entry) after 48h. Alternatively, after gentamicin treatment and washing, RPMI (or DMEM) containing 10% HI-FBS was added to cells and they were incubated for 6 or 24 h, lysed, serially-diluted, and plated to determine bacterial numbers.

Expression and Purification of Recombinant FTL1678 and FTT0101. *F. tularensis* LVS and SchuS4 genomic DNA were extracted using phenol/chloroform/isoamyl alcohol (Fisher Bioreagents). *FTL1678* and *FTT0101*, without signal sequences (amino acid residues 1-29), were PCR-amplified from LVS and SchuS4 genomic DNA, respectively, using High Fidelity Platinum Taq Polymerase (Life Technologies), and primers 5'FTL1678_BamHI and 3'FTL1678_XhoI and 5'FTT0101_BamHI and 3'FTT0101_XhoI, respectively (Table S2). Amplicons and pPROEX HTb were double-digested with BamHI and XhoI, ligated using T4 DNA ligase, and transformed into NEB 10-β *E. coli*. Plasmids were purified using the Qiagen QIAprep Spin Miniprep kit and diagnostic PCR was performed to confirm presence and correct size of the insert. DNA sequencing was performed to confirm insert integrity and plasmid constructs were transformed into Rosetta DE3 *E. coli* (Millipore) for protein expression. Recombinant proteins were expressed and purified as previously described (24) with some modifications. Bacteria were grown in LB-amp to an OD_{600} of 0.4, protein expression was induced for 2 h by the addition of isopropyl β-D-thiogalactopyranoside (IPTG) to a final concentration of 100 mM, bacteria were pelleted by centrifugation, and frozen overnight at −80°C to aid in lysis. Cell pellets were suspended in 10 mM Tris, 500 mM NaCl, and 10 mM imidazole, pH 8.0, sonicated on ice for 10 min with 30 sec intervals, insoluble material was removed by centrifugation at 8,000 × *g*, and supernatants were collected for affinity purification

over pre-equilibrated Ni-nitrilotriacetic acid (Ni-NTA) agarose (Qiagen) columns. Eluted recombinant proteins were concentrated in Amicon Ultra-4 centrifugal filter units with 30-kDa cutoff (Millipore), concentrations were determined using the DC BCA protein assay (BioRad), and purity was assessed by SDS-PAGE and Imperial protein staining (Thermo Scientific). An empty vector construct also was expressed and purified as a control in enzymatic assays.

Enzymatic Assays for FTL1678/FTT0101 Activity. FTL1678 and FTT0101 recombinant protein activity toward various PG-related compounds were tested in 50 µl reaction mixtures containing 50 mM Tris-HCl, pH 8.0, 0.1 mM substrate, and partially purified enzyme stock (10 µl in 1 M NaCl, 10 mM Tris, pH 8.0). Mixtures were incubated for 30 min to 2 h at 37°C and reactions were stopped by freezing. Substrate and reaction products were separated by HPLC on an ODS-Hypersil 3 µm particle-size C18 column (250 by 4.6 mm; Thermo Scientific). Elutions were performed with 50 mM sodium phosphate buffer, pH 4.5, with or without application of a linear gradient of methanol (from 0 to 50% in 50 min), at a flow rate of 0.5 ml/min. Peaks were detected by measuring the absorbance at 207 nm or at 262 nm for UDP-containing nucleotide precursors. Identification of compounds was based on their retention times, compared to authentic standards, as well as on their amino acid and amino sugar composition, determined with a Hitachi model L8800 analyzer (Sciencetec) after hydrolysis of samples in 6 M HCl for 16 h at 95°C. Enzyme activity was calculated by integration of peaks corresponding to substrate and product. Amounts of alanine released by the L,D-carboxypeptidase activity also were determined using an amino acid analyzer. Depending on the substrate used, the amount of partially purified protein varied from 0.9 to 5 µg per assay and incubation times varied from 30 min to 4 h. To ensure linearity, substrate consumption was <

20% in all cases. Values represent the means for three independent experiments; the standard deviation was < 10% in all cases. Specific activities were calculated from the amounts of D-Ala (tetrapeptide substrates) or D-Ala-D-Ala (pentapeptide substrates) released during the reaction.

Peptidoglycan Precursors and Muropeptides. UDP-MurNAc-pentapeptide precursors containing either *meso*-diaminopimelic acid (A_2pm) or L-lysine were prepared by enzymatic synthesis using purified Mur ligases, and UDP-MurNAc-tetrapeptides were generated by treatment of the UDP-MurNAc-pentapeptide precursors with purified *E. coli* PBP5 DD-carboxypeptidase as previously described (68). MurNAc-peptides were obtained by mild acid hydrolysis of UDP-MurNAc-peptides (0.1 M HCl, 100°C, 15 min) and were not reduced and thus purified as a mixture of the two α and β anomers (69). Free peptides were prepared by cleavage of MurNAc-peptides with *E. coli* AmiD *N*-acetylmuramoyl-L-alanine amidase (70). The *E. coli* peptidoglycan polymer was purified from a Δ*lpp* mutant strain that does not express the Lpp lipoprotein (71). GlcNAc-1,6-anhydro-MurNAc-L-Ala-γ-D-Glu-*meso*-A_2pm-D-Ala (TCT) and its dimer (two cross-linked TCT monomers) were produced by digestion of peptidoglycan with *E. coli* SltY lytic transglycosylase and the non-anhydro forms of these monomer and dimer were generated by digestion of the polymer with mutanolysin (72). All these compounds were HPLC-purified and their composition was controlled by amino acid and amino sugar content analysis and/or by MALDI-TOF mass spectrometry.

Statistics. GraphPad Prism6 was used in various statistical analyses, including: differences in antibiotic, detergent, dye, or lysozyme susceptibility were calculated by one-way ANOVA with multiple comparisons and the Holm-Sidak post-hoc test; differences in EM

measurements were determined by unpaired t-tests; differences in median time-to-death and percent survival following *F. tularensis* infection of mice were calculated using the log-rank Mantel-Cox test; differences in pathology scores of *F. tularensis*-infected tissues were calculated by two-way ANOVA with multiple comparisons and a Tukey post-hoc test. Differences in lung, liver, spleen, and blood bacterial burdens from infected mice were calculated by one-way ANOVA with multiple comparisons using R software.

References

1. Dhar S, Kumari H, Balasubramanian D, Mathee K. 2018. Cell-wall recycling and synthesis in *Escherichia coli* and *Pseudomonas aeruginosa* - their role in the development of resistance. *J Med Microbiol* **67**:1-21.
2. Johnson J, Fisher JF, Mobashery S. 2013. Bacterial cell-wall recycling. *Ann N Y Acad Sci* **1277**:54-75.
3. Mengin-Lecreulx D, Lemaitre B. 2005. Structure and metabolism of peptidoglycan and molecular requirements allowing its detection by the Drosophila innate immune system. *J Endotoxin Res* **11**:105-11.
4. Braun V, Rehn K. 1969. Chemical characterization, spatial distribution and function of a lipoprotein (murein-lipoprotein) of the E. coli cell wall. The specific effect of trypsin on the membrane structure. *Eur J Biochem* **10**:426-38.
5. Braun V. 1975. Covalent lipoprotein from the outer membrane of Escherichia coli. *Biochim Biophys Acta* **415**:335-77.
6. Bouveret E, Benedetti H, Rigal A, Loret E, Lazdunski C. 1999. In vitro characterization of peptidoglycan-associated lipoprotein (PAL)-peptidoglycan and PAL-TolB interactions. *J Bacteriol* **181**:6306-11.
7. Leduc M, Ishidate K, Shakibai N, Rothfield L. 1992. Interactions of Escherichia coli membrane lipoproteins with the murein sacculus. *J Bacteriol* **174**:7982-8.
8. Glauner B, Holtje JV, Schwarz U. 1988. The composition of the murein of Escherichia coli. *J Biol Chem* **263**:10088-95.
9. Pazos M, Peters K. 2019. Peptidoglycan. *Subcell Biochem* **92**:127-168.

10. Typas A, Banzhaf M, Gross CA, Vollmer W. 2011. From the regulation of peptidoglycan synthesis to bacterial growth and morphology. *Nat Rev Microbiol* **10**:123-36.

11. Park J, Uehara T. 2008. How bacteria consume their own exoskeletons (turnover and recycling of cell wall peptidoglycan). *Microbiol Mol Biol Rev* **72**:211-27.

12. Holtje J. 1998. Growth of the stress-bearing and shape-maintaining murein sacculus of Escherichia coli. *Microbiol Mol Biol Rev* **62**:181-203.

13. Juan C, Torrens G, Barcelo IM, Oliver A. 2018. Interplay between Peptidoglycan Biology and Virulence in Gram-Negative Pathogens. *Microbiol Mol Biol Rev* **82**:e00033-18.

14. Russo T, MacDonald U, Beanan JM, Olson R, MacDonald IJ, Sauberan SL, Luke NR, Schultz LW, Umland TC. 2009. Penicillin-binding protein 7/8 contributes to the survival of Acinetobacter baumannii in vitro and in vivo. *J Infect Dis* **199**:513-21.

15. Chaput C, Ecobichon C, Pouradier N, Rousselle JC, Namane A, Boneca IG. 2016. Role of the N-Acetylmuramoyl-l-Alanyl Amidase, AmiA, of Helicobacter pylori in Peptidoglycan Metabolism, Daughter Cell Separation, and Virulence. *Microb Drug Resist* **22**:477-86.

16. Scheurwater E, Reid CW, Clarke AJ. 2008. Lytic transglycosylases: bacterial space-making autolysins. *Int J Biochem Cell Biol* **40**:586-91.

17. Dennis D, Inglesby TV, Henderson DA, Bartlett JG, Ascher MS, Eitzen E, Fine AD, Friedlander AM, Hauer J, Layton M, Lillibridge SR, McDade JE, Osterholm MT, O'Toole T, Parker G, Perl TM, Russell PK, and Tonat K. 2001. Tularemia as a biological weapon: medical and public health management. *JAMA* **285**:2763-73.

18. Keim P, Johansson A, Wagner DM. 2007. Molecular epidemiology, evolution, and ecology of Francisella. *Ann N Y Acad Sci* **1105**:30-66.

19. Kingry L, Petersen JM. 2014. Comparative review of Francisella tularensis and Francisella novicida. *Front Cell Infect Microbiol* **4**:35.

20. Ellis J, Oyston PC, Green M, Titball RW. 2002. Tularemia. *Clin Microbiol Rev* **15**:631-46.

21. Sjostedt A. 2007. Tularemia: history, epidemiology, pathogen physiology, and clinical manifestations. *Ann N Y Acad Sci* **1105**:1-29.

22. Ray K, Marteyn B, Sansonetti PJ, Tang CM. 2009. Life on the inside: the intracellular lifestyle of cytosolic bacteria. *Nat Rev Microbiol* **7**:333-40.

23. Jones C, Napier BA, Sampson TR, Llewellyn AC, Schroeder MR, Weiss DS. 2012. Subversion of host recognition and defense systems by Francisella spp. *Microbiol Mol Biol Rev* **76**:383-404.

24. Ren G, Champion MM, Huntley JF. 2014. Identification of disulfide bond isomerase substrates reveals bacterial virulence factors. *Mol Microbiol* **94**:926-44.

25. Qin A, Scott DW, Thompson JA, Mann BJ. 2009. Identification of an essential Francisella tularensis subsp. tularensis virulence factor. *Infect Immun* **77**:152-61.

26. Metz R, Henning S, Hammes WP. 1986. LD-carboxypeptidase activity in Escherichia coli. I. The LD-carboxypeptidase activity in ether treated cells. *Arch Microbiol* **144**:175-80.

27. Templin M, Ursinus A, Holtje JV. 1999. A defect in cell wall recycling triggers autolysis during the stationary growth phase of Escherichia coli. *EMBO J* **18**:4108-17.

28. Metz R, Henning S, Hammes WP. 1986. LD-carboxypeptidase activity in Escherichia coli. II. Isolation, purification and characterization of the enzyme from E. coli K 12. *Arch Microbiol* **144**:181-6.

29. Ursinus A, Steinhaus H, Holtje JV. 1992. Purification of a nocardicin A-sensitive LD-carboxypeptidase from Escherichia coli by affinity chromatography. *J Bacteriol* **174**:441-6.

30. Korza H, Bochtler M. 2005. Pseudomonas aeruginosa LD-carboxypeptidase, a serine peptidase with a Ser-His-Glu triad and a nucleophilic elbow. *J Biol Chem* **280**:40802-12.

31. Lenz J, Hackett KT, Dillard JP. 2017. A Single Dual-Function Enzyme Controls the Production of Inflammatory NOD Agonist Peptidoglycan Fragments by Neisseria gonorrhoeae. *MBio* **8**:e01464-17.

32. Frirdich E, Vermeulen J, Biboy J, Soares F, Taveirne ME, Johnson JG, DiRita VJ, Girardin SE, Vollmer W, Gaynor EC. 2014. Peptidoglycan LD-carboxypeptidase Pgp2 influences Campylobacter jejuni helical cell shape and pathogenic properties and provides the substrate for the DL-carboxypeptidase Pgp1. *J Biol Chem* **289**:8007-18.

33. Rashid Y, Kamran Azim M. 2011. Structural bioinformatics of Neisseria meningitidis LD-carboxypeptidase: implications for substrate binding and specificity. *Protein J* **30**:558-65.

34. Huntley J, Conley PG, Hagman KE, Norgard MV. 2007. Characterization of Francisella tularensis outer membrane proteins. *J Bacteriol* **189**:561-74.

35. Clavel T, Germon P, Vianney A, Portalier R, Lazzaroni JC. 1998. TolB protein of Escherichia coli K-12 interacts with the outer membrane peptidoglycan-associated proteins Pal, Lpp and OmpA. *Mol Microbiol* **29**:359-67.

36. Walburger A, Lazdunski C, Corda Y. 2002. The Tol/Pal system function requires an interaction between the C-terminal domain of TolA and the N-terminal domain of TolB. *Mol Microbiol* **44**:695-708.

37. Sycuro L, Rule CS, Petersen TW, Wyckoff TJ, Sessler T, Nagarkar DB, Khalid F, Pincus Z, Biboy J, Vollmer W, Salama NR. 2013. Flow cytometry-based enrichment for cell shape mutants identifies multiple genes that influence Helicobacter pylori morphology. *Mol Microbiol* **90**:869-83.

38. Nelson D, Young KD. 2000. Penicillin binding protein 5 affects cell diameter, contour, and morphology of Escherichia coli. *J Bacteriol* **182**:1714-21.

39. Guinane C, Cotter PD, Ross RP, Hill C. 2006. Contribution of penicillin-binding protein homologs to antibiotic resistance, cell morphology, and virulence of Listeria monocytogenes EGDe. *Antimicrob Agents Chemother* **50**:2824-8.

40. Priyadarshini R, de Pedro MA, Young KD. 2007. Role of peptidoglycan amidases in the development and morphology of the division septum in Escherichia coli. *J Bacteriol* **189**:5334-47.

41. Heidrich C, Templin MF, Ursinus A, Merdanovic M, Berger J, Schwarz H, de Pedro MA, Holtje JV. 2001. Involvement of N-acetylmuramyl-L-alanine amidases in cell separation and antibiotic-induced autolysis of Escherichia coli. *Mol Microbiol* **41**:167-78.

42. Sycuro L, Pincus Z, Gutierrez KD, Biboy J, Stern CA, Vollmer W, Salama NR. 2010. Peptidoglycan crosslinking relaxation promotes Helicobacter pylori's helical shape and stomach colonization. *Cell* **141**:822-33.

43. Wu X, Ren G, Gunning WT 3rd, Weaver DA, Kalinoski AL, Khuder SA, Huntley JF. 2016. FmvB: A Francisella tularensis Magnesium-Responsive Outer Membrane Protein that Plays a Role in Virulence. *PLoS One* **11**:e0160977.

44. Heidrich C, Ursinus A, Berger J, Schwarz H, Holtje JV. 2002. Effects of multiple deletions of murein hydrolases on viability, septum cleavage, and sensitivity to large toxic molecules in Escherichia coli. *J Bacteriol* **184**:6093-9.

45. Denome S, Elf PK, Henderson TA, Nelson DE, Young KD. 1999. Escherichia coli mutants lacking all possible combinations of eight penicillin binding proteins: viability, characteristics, and implications for peptidoglycan synthesis. *J Bacteriol* **181**:3981-93.

46. Priyadarshini R, Popham DL, Young KD. 2006. Daughter cell separation by penicillin-binding proteins and peptidoglycan amidases in Escherichia coli. *J Bacteriol* **188**:5345-55.

47. Meyer K, Addy C, Akashi S, Roper DI, Tame JRH. 2018. The crystal structure and oligomeric form of Escherichia coli L,D-carboxypeptidase A. *Biochem Biophys Res Commun* **499**:594-599.

48. Das D, Herve M, Elsliger MA, Kadam RU, Grant JC, Chiu HJ, Knuth MW, Klock HE, Miller MD, Godzik A, Lesley SA, Deacon AM, Mengin-Lecreulx D, Wilson IA. 2013. Structure and function of a novel LD-carboxypeptidase a involved in peptidoglycan recycling. *J Bacteriol* **195**:5555-66.

49. De Pascalis R, Hahn A, Brook HM, Ryden P, Donart N, Mittereder L, Frey B, Wu TH, Elkins KL. 2018. A panel of correlates predicts vaccine-induced protection of rats against respiratory challenge with virulent Francisella tularensis. *PLoS One* **13**:e0198140.

50. Steiner D, Furuya Y, Jordan MB, Metzger DW. 2017. Protective Role for Macrophages in Respiratory Francisella tularensis Infection. *Infect Immun* **85**.

51. Hall J, Woolard MD, Gunn BM, Craven RR, Taft-Benz S, Frelinger JA, Kawula TH. 2008. Infected-host-cell repertoire and cellular response in the lung following inhalation of Francisella tularensis Schu S4, LVS, or U112. *Infect Immun* **76**:5843-52.

52. Minor P. 2015. Live attenuated vaccines: Historical successes and current challenges. *Virology* **479-480**:379-92.

53. Roberts L, Powell DA, Frelinger JA. 2018. Adaptive Immunity to Francisella tularensis and Considerations for Vaccine Development. *Front Cell Infect Microbiol* **8**:115.

54. de Pedro M, Cava F. 2015. Structural constraints and dynamics of bacterial cell wall architecture. *Front Microbiol* **6**:449.

55. den Blaauwen T, de Pedro MA, Nguyen-Disteche M, Ayala JA. 2008. Morphogenesis of rod-shaped sacculi. *FEMS Microbiol Rev* **32**:321-44.

56. Silhavy TJ, Kahne D, Walker S. 2010. The bacterial cell envelope. *Cold Spring Harb Perspect Biol* **2**:a000414.

57. van Heijenoort J. 2011. Peptidoglycan hydrolases of Escherichia coli. *Microbiol Mol Biol Rev* **75**:636-63.

58. Jenkins C, Wallis R, Allcock N, Barnes KB, Richards MI, Auty JM, Galyov EE, Harding SV, Mukamolova GV. 2019. The lytic transglycosylase, LtgG, controls cell morphology and virulence in Burkholderia pseudomallei. *Sci Rep* **9**:11060.

59. Spidlova P, Stojkova P, Dankova V, Senitkova I, Santic M, Pinkas D, Philimonenko V, Stulik J. 2018. Francisella tularensis D-Ala D-Ala Carboxypeptidase DacD Is Involved in

Intracellular Replication and It Is Necessary for Bacterial Cell Wall Integrity. *Front Cell Infect Microbiol* **8**:111.

60. Kijek T, Mou S, Bachert BA, Kuehl KA, Williams JA, Daye SP, Worsham PL, Bozue JA. 2019. The D-alanyl-d-alanine carboxypeptidase enzyme is essential for virulence in the Schu S4 strain of Francisella tularensis and a dacD mutant is able to provide protection against a pneumonic challenge. *Microb Pathog* **137**:103742.

61. Lenz JD, Hackett KT, Dillard JP. 2017. A Single Dual-Function Enzyme Controls the Production of Inflammatory NOD Agonist Peptidoglycan Fragments by Neisseria gonorrhoeae. *MBio* **8**.

62. Wu X, Ren G, Huntley JF. 2015. Generating Isogenic Deletions (Knockouts) in Francisella tularensis, a Highly-infectious and Fastidious Gram-negative Bacterium. *Bio Protoc* **5**:e1500.

63. Gallagher L, McKevitt M, Ramage ER, Manoil C. 2008. Genetic dissection of the Francisella novicida restriction barrier. *J Bacteriol* **190**:7830-7.

64. Robertson G, Child R, Ingle C, Celli J, Norgard MV. 2013. IglE is an outer membrane-associated lipoprotein essential for intracellular survival and murine virulence of type A Francisella tularensis. *Infect Immun* **81**:4026-40.

65. Maier T, Havig A, Casey M, Nano FE, Frank DW, Zahrt TC. 2004. Construction and characterization of a highly efficient Francisella shuttle plasmid. *Appl Environ Microbiol* **70**:7511-9.

66. Huntley J, Conley PG, Rasko DA, Hagman KE, Apicella MA, Norgard MV. 2008. Native outer membrane proteins protect mice against pulmonary challenge with virulent type A Francisella tularensis. *Infect Immun* **76**:3664-71.

67. Price C. 1982. Centrifugation in density gradients. *Academic Press*:335-343.

68. Herve M, Boniface A, Gobec S, Blanot D, Mengin-Lecreulx D. 2007. Biochemical characterization and physiological properties of Escherichia coli UDP-N-acetylmuramate:L-alanyl-gamma-D-glutamyl-meso-diaminopimelate ligase. *J Bacteriol* **189**:3987-95.

69. Blanot D, Kretsovali A, Abo-Ghalia M, Mengin-Lecreulx D, van Heijenoort J. 1983. Synthesis of analogues of precursors of bacterial peptidoglycan, p 311-314. *In* Malon BaP (ed), Peptides. Walter de Gruyter, Berlin, Germany.

70. Pennartz A, Genereux C, Parquet C, Mengin-Lecreulx D, Joris B. 2009. Substrate-induced inactivation of the Escherichia coli AmiD N-acetylmuramoyl-L-alanine amidase highlights a new strategy to inhibit this class of enzyme. *Antimicrob Agents Chemother* **53**:2991-7.

71. Leulier F, Parquet C, Pili-Floury S, Ryu JH, Caroff M, Lee WJ, Mengin-Lecreulx D, Lemaitre B. 2003. The Drosophila immune system detects bacteria through specific peptidoglycan recognition. *Nat Immunol* **4**:478-84.

72. Stenbak C, Ryu JH, Leulier F, Pili-Floury S, Parquet C, Herve M, Chaput C, Boneca IG, Lee WJ, Lemaitre B, Mengin-Lecreulx D. 2004. Peptidoglycan molecular requirements allowing detection by the Drosophila immune deficiency pathway. *J Immunol* **173**:7339-48.

Table 1: Specific Activity and Substrate Specificity of the FTL1678/FTT0101 Enzymes[a]

Substrate	Specific Activity (nmol/min/mg of protein) [a]	
	FTL1678	FTT0101
A_2pm-containing substrates		
GlcNAc-anhydroMurNAc-L-Ala-γ-D-Glu-*meso*-A_2pm-D-Ala (TCT)	21.5	29.0
GlcNAc-MurNAc-L-Ala-γ-D-Glu-*meso*- A_2pm-D-Ala (PG monomer)	15.6	24.2
TCT dimer	7.7	11.8
MurNAc-L-Ala-γ-D-Glu-*meso*-A2pm-D-Ala	5.8	7.8
UDP-MurNAc-L-Ala-γ-D-Glu-*meso*-A_2pm-D-Ala	4.6	6.3
L-Ala-γ-D-Glu-*meso*-A_2pm-D-Ala (free tetrapeptide)	3.4	8.0
MurNAc-L-Ala-γ-D-Glu-*meso*-A_2pm-D-Ala-D-Ala (pentapeptide)	9.8	6.2
UDP-MurNAc-L-Ala-γ-D-Glu-*meso*-A_2pm-D-Ala-D-Ala (pentapeptide)	5.9	6.4
L-Lysine-containing substrates		
MurNAc-L-Ala-γ-D-Glu-L-Lys-D-Ala	1.3	2.1
L-Ala-γ-D-Glu-L-Lys-D-Ala	0.7	2.1
UDP-MurNAc-L-Ala-γ-D-Glu-L-Lys-D-Ala-D-Ala	1.2	1.7
Other		
GlcNAc-MurNAc-L-Ala-γ-D-Glu-*meso*-A_2pm(NH_2)-D-Ala		Very low (<0.5)
GlcNAc-MurNAc-L-Ala-γ-D-Glu(NH_2)-*meso*-A_2pm-D-Ala		Not detected [b]
GlcNAc-MurNAc-L-Ala-γ-D-Glu(NH_2)-*meso*-A_2pm(NH_2)-D-Ala		Not detected [b]
Peptidoglycan polymer		Not detected [b]

[a] The standard enzyme assay conditions are described in the Materials and Methods.

[b] Not detected means that no release of alanine could be detected.

994 Table 2 : Sensitivity of WT and Δ*FTL1678* to antibiotics, detergents, and dyes

Compound	Concentration (μg/disk)	Average Zone of Inhibition, mm (mean ± SD)	
		WT	ΔFTL1678
Gentamicin	4	2.50 ± 0.10	0.93 ± 0.15 R
Tetracycline	5	1.83 ± 0.06	0.80 ± 0.00 R
Chloramphenicol	5	3.37 ± 0.12	1.00 ± 0.00 R
Ciprofloxacin	5	4.73 ± 0.23	1.90 ± 0.10 R
Ampicillin	200	2.57 ± 0.12	3.53 ± 0.15 S
Vancomycin	20	1.27 ± 0.21	2.60 ± 0.10 S
Bacitracin	182	1.10 ± 0.10	1.20 ± 0.10
Polymyxin B	100	0.70 ± 0.00	0.70 ± 0.00
Lysozyme	1000	0.70 ± 0.00	1.67 ± 0.06 S
Ethidium Bromide	5	2.73 ± 0.15	0.80 ± 0.00 R
Triton-X 100	750	3.40 ± 0.27	2.63 ± 0.06 R
SDS	1000	1.20 ± 0.10	1.80 ± 0.00 S
CTAB	50	0.73 ± 0.06	0.80 ± 0.10
CHAPS	50	0.70 ± 0.00	0.70 ± 0.00

995

996 R indicates Δ*FTL1678* is significantly more resistant than WT by one-way ANOVA ($P<0.05$)

997 S indicates Δ*FTL1678* is significantly more sensitive than WT by one-way ANOVA ($P<0.05$)

Fig 1. Amino acid alignment of bacterial L,D-carboxypeptidases. Clustal Omega amino acid alignment of *E. coli* LdcA (BAA36050.1), *P. aeruginosa* LdcA (Q9HTZ1), *N. gonorrhoeae* LdcA (YP_208343.1), *F. tularensis* Type B FTL1678, and *F. tularensis* Type A FTT0101, and *C. jejuni* Pgp2 (WP_002856863). Percent identities (pid), compared to *E. coli* LdcA, are indicated. Black shading indicates similar residues. Red shading indicates the catalytic triad.

Fig 2. FTL1678 is OM-associated. Spheroplasting, osmotic lysis, and sucrose density gradient centrifugation were performed to separate inner membranes (IM) and outer membranes (OM) from *F. tularensis* ΔFTL1678 *trans*-complemented with a 6× histidine-tagged FTL1678. Whole-cell lysates (WCL), OM fractions, and IM fractions were separated by SDS-PAGE, transferred to nitrocellulose, and immunoblotting was performed using antisera specific for the OM control protein FopA (αFopA), IM control protein SecY (αSecY), or histidine-tagged FTL1678.

Fig 3. *F. tularensis* Δ*FTL1678* has altered cell morphology. Electron micrograph images of: (A) wild-type LVS [WT] or (B) Δ*FTL1678* grown in sMHB to OD_{600} of 0.4. Scale bars represent 100 nm; (C) Outer membrane thickness measurements [nm] were measured for WT and Δ*FTL1678*, n=50; (D) Cell width measurements [nm] for WT and Δ*FTL1678*, n=175. ****$P<0.0001$

Fig 4. Susceptibility of *F. tularensis* WT LVS and Δ*FTL1678* to stressors. WT and Δ*FTL1678* were grown in 75 ml sMHB at: (A) 37˚C, (B) sMHB at 40˚C, (C) sMHB + 60 μM $CuCl_2$, (D) sMHB + 5 mM H_2O_2, (E) sMHB + 5% NaCl, or (F) sMHB at pH 5.5. Bacteria were grown for 24 hours and OD_{600} measurements were recorded every 4 hours.

Fig 5. FTL1678 and Ldc activity are required for *F. tularensis* virulence. (A) Groups of 5 C3H/HeN mice were intranasally-infected with 10^5 CFU of either wild-type WT, Δ*FTL1678*, or the FTL1678 *trans*-complement [FTL1678 compl]. Animal health was monitored daily through day 21 post-infection. **** $P<0.0001$; (B) Lungs, livers, spleens, and blood were aseptically harvested from mice infected with 10^4 CFU of either WT or Δ*FTL1678* on days 2 and 5 post-infection and plated to enumerate bacterial numbers. *$P<0.01$; (C) Groups of 5 C3H/HeN mice were intranasally-infected with 10^5 CFU of either LVS, Δ*FTL1678*, FTL1678 *trans*-complement [FTL1678 compl], or *C. jejuni* Pgp2 *trans*-complement [Pgp2 compl]. Animal health was monitored through day 21 post-infection. ** $P<0.01$

Fig 6. FTL1678 is required for *F. tularensis* replication in macrophages. (A) J774A.1 macrophages or mouse bone marrow-derived macrophages (mBMDMs) were infected with WT or Δ*FTL1678* at an MOI of 100:1 and bacterial numbers were enumerated at entry (0 h), 6 h, and 24 h post-infection. (B) Fold change in bacterial numbers from 6 to 24 h post-infection was calculated. * $P< 0.01$

Fig 7. Δ*FTL1678* protects against fully-virulent Type A *F. tularensis* SchuS4. (A) Groups of 5 C3H/HeN mice were intranasally infected with either 10^5 CFU WT or 10^5, 10^7, or 10^9 CFU Δ*FTL1678*. On day 29 post-infection, mice were boosted with 10^9 CFU Δ*FTL1678* and animal health was monitored daily through day 50 post-infection. *** $P<0.001$; (B) Mice from A were intranasally-challenged with 120 CFU of wild-type SchuS4 [BSL3; 6× LD50]. Animal health was monitored daily through day 26 post-infection. *$P<0.001$

Fig 8. Δ*FTL1678* does not induce pathology. (A) Hematoxylin and eosin (H&E)-stained tissues were examined from either uninfected, *F. tularensis* WT LVS-, or Δ*FTL1678*-infected mice at 10× objective. (B) Tissues were graded on a scale of 0 to 4 with 4 being the most severe. *$P<0.05$

Fig. 9. Peptidoglycan synthesis and recycling pathways remain to be defined in *F. tularensis.* Bioinformatic analyses were used to identify proteins that may be involved in peptidoglycan synthesis and recycling in *F. tularensis* LVS. Locus tags are indicated.

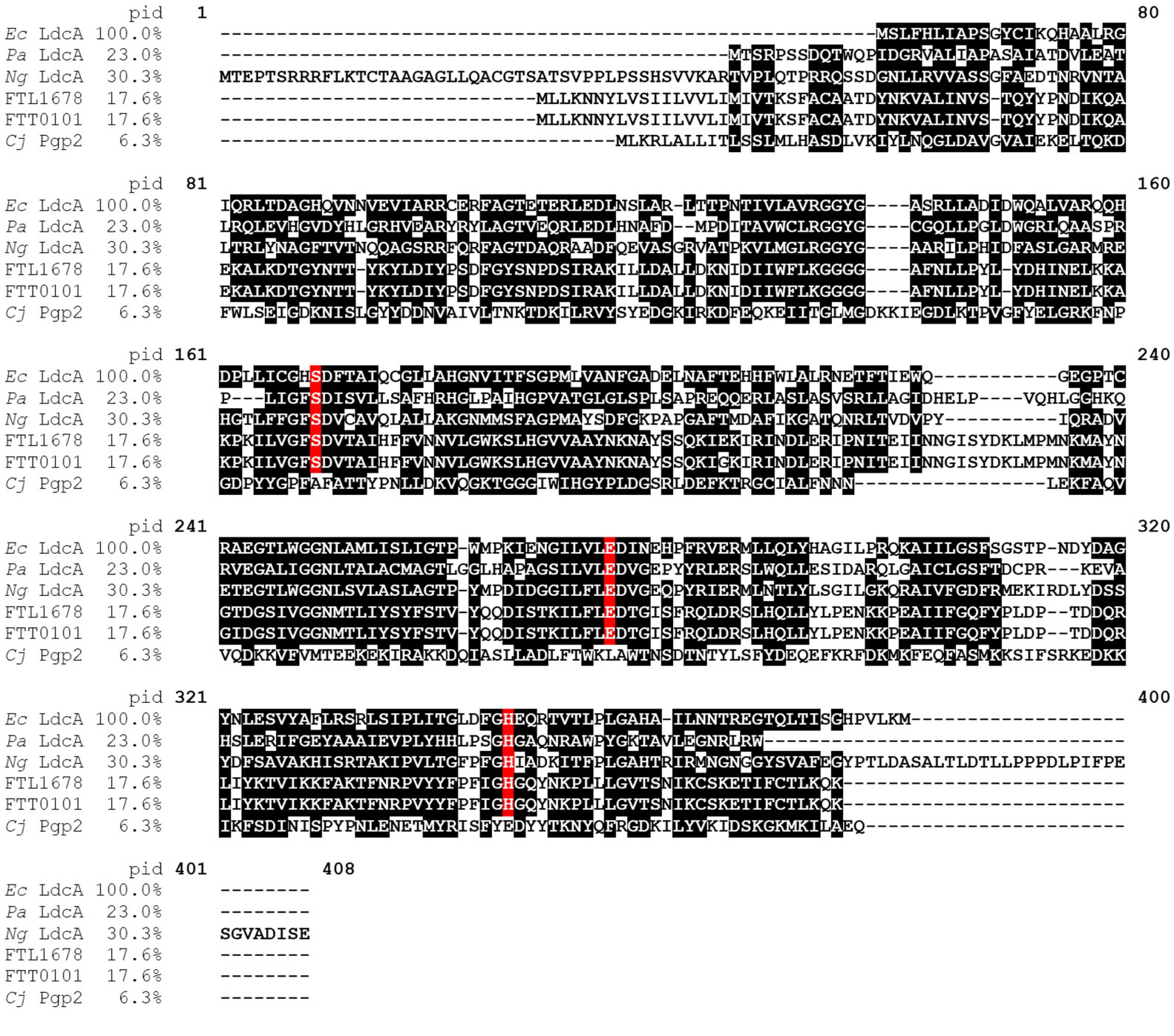

Fig 1. Amino acid alignment of bacterial L,D-carboxypeptidases. Clustal Omega amino acid alignment of *E. coli* LdcA (BAA36050.1), *P. aeruginosa* LdcA (Q9HTZ1), *N. gonorrhoeae* LdcA (YP_208343.1), *F. tularensis* Type B FTL1678, *F. tularensis* Type A FTT0101, and *C. jejuni* Pgp2 (WP_002856863). Percent identities (pid), compared to *E. coli* LdcA, are indicated. Black shading indicates similar residues. Red shading indicates the catalytic triad.

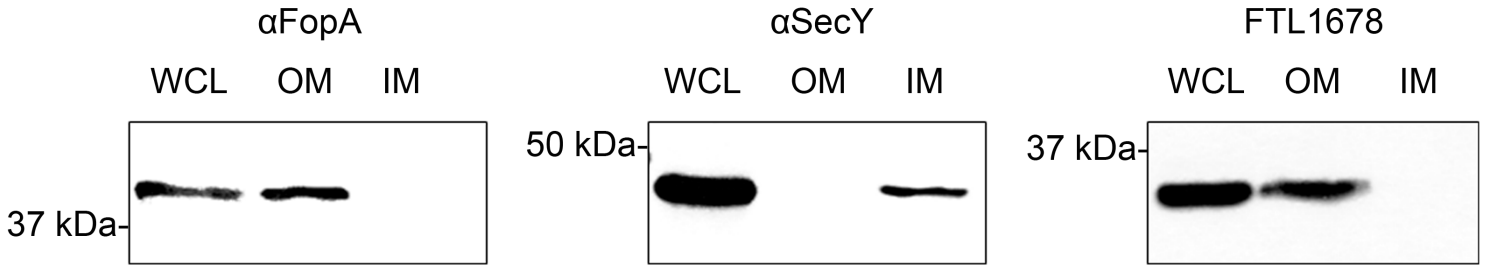

Fig 2. FTL1678 is OM-associated. Spheroplasting, osmotic lysis, and sucrose density gradient centrifugation were performed to separate inner membranes (IM) and outer membranes (OM) from *F. tularensis* Δ*FTL1678 trans*-complemented with a 6x histidine-tagged FTL1678. Whole-cell lysates (WCL), OM fractions, and IM fractions were separated by SDS-PAGE, transferred to nitrocellulose, and immunoblotting was performed using antisera specific for the OM control protein FopA (αFopA), IM control protein SecY (αSecY), or histidine-tagged FTL1678.

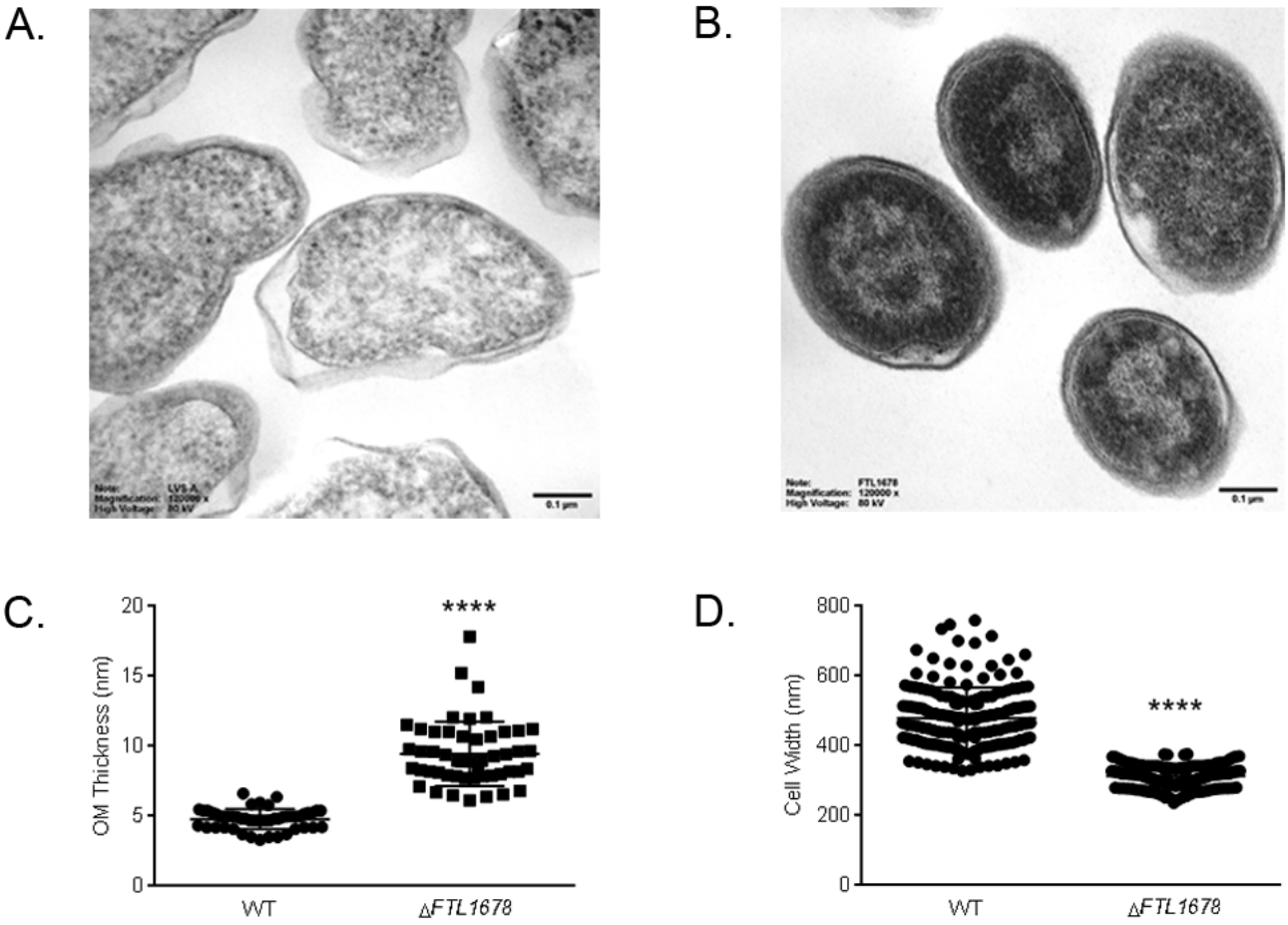

Fig 3. *F. tularensis* Δ*FTL1678* has altered cell morphology. Electron micrograph images of: (A) wild-type LVS [WT] or (B) Δ*FTL1678* grown in sMHB to OD_{600} of 0.4. Scale bars represent 100 nm; (C) Outer membrane thickness measurements [nm] were measured for WT and Δ*FTL1678*, n=50; (D) Cell width measurements [nm] for WT and ΔFTL1678, n=175. ****$P<0.0001$

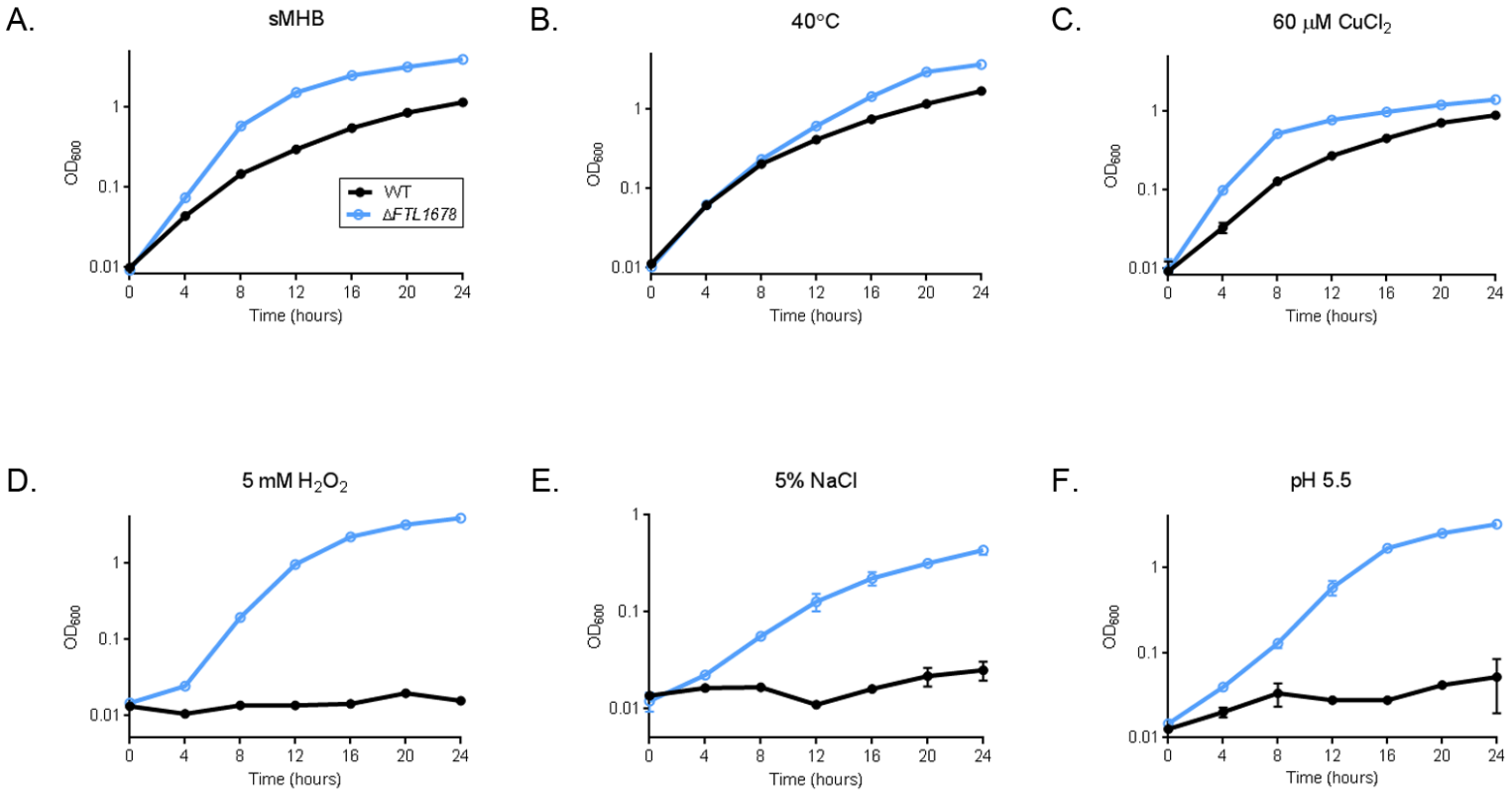

Fig 4. Susceptibility of *F. tularensis* WT LVS and Δ*FTL1678* to stressors. WT and Δ*FTL1678* were grown in 75 ml sMHB at: (A) 37˚C, (B) 40˚C, (C) with 60 μM $CuCl_2$, (D) with 5 mM H_2O_2, (E) with 5% NaCl, or (F) at pH 5.5. Bacteria were grown for 24 hours and OD_{600} measurements were recorded every 4 hours.

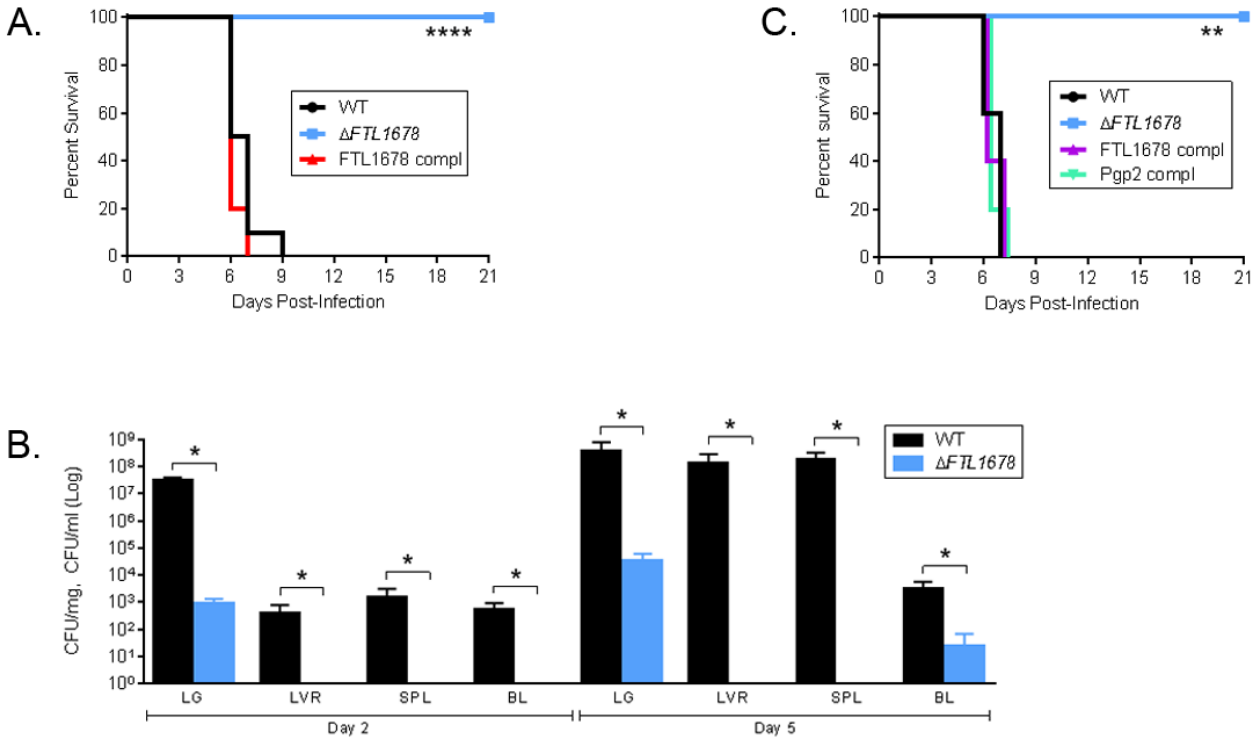

Fig 5. FTL1678 and Ldc activity are required for *F. tularensis* virulence. (A) Groups of 5 C3H/HeN mice were intranasally-infected with 10^5 CFU of either wild-type WT, Δ*FTL1678*, or the FTL1678 *trans*-complement [FTL1678 compl]. Animal health was monitored daily through day 21 post-infection. **** $P<0.0001$; (B) Lungs, livers, spleens, and blood were aseptically harvested from mice infected with 10^4 CFU of either WT or Δ*FTL1678* on days 2 and 5 post-infection and plated to enumerate bacterial numbers. *$P<0.01$; (C) Groups of 5 C3H/HeN mice were intranasally-infected with 10^5 CFU of either LVS, Δ*FTL1678*, FTL1678 *trans*-complement [FTL1678 compl], or *C. jejeuni* Pgp2 *trans*-complement [Pgp2 compl]. Animal health was monitored through day 21 post-infection. ** $P<0.01$

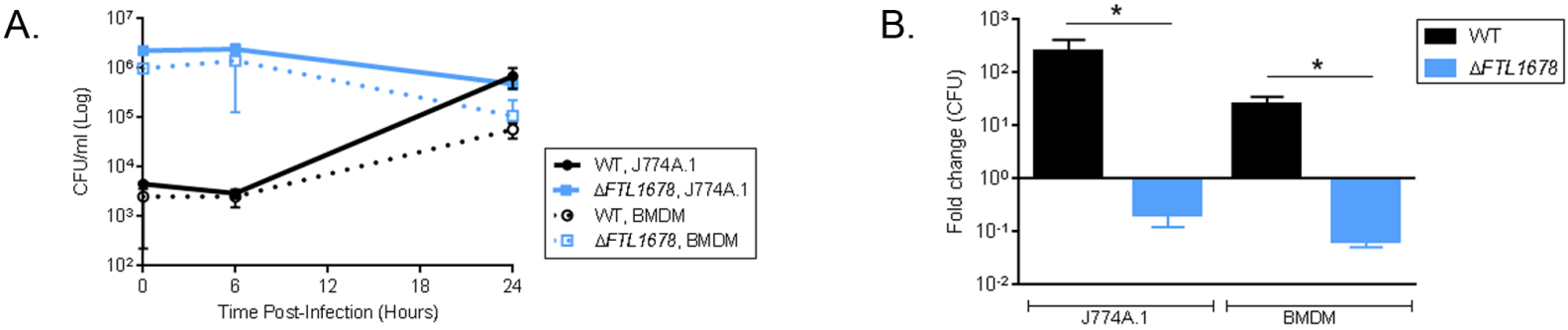

Fig 6. FTL1678 is required for *F. tularensis* replication in macrophages. (A) J774A.1 macrophages or mouse bone marrow-derived macrophages (mBMDMs) were infected with WT or Δ*FTL1678* at an MOI of 100:1 and bacterial numbers were enumerated at entry (0 h), 6 h, and 24 h post-infection. (B) Fold change in bacterial numbers from 6 to 24 h post-infection was calculated. * $P < 0.01$

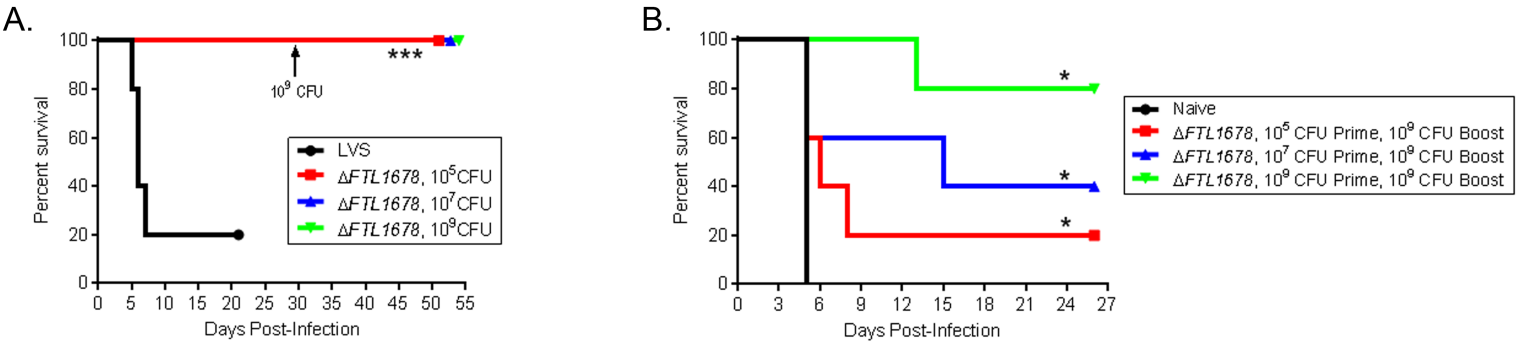

Fig 7. Δ*FTL1678* protects against fully-virulent Type A *F. tularensis* SchuS4. (A) Groups of 5 C3H/HeN mice were intranasally infected with either 10^5 CFU WT or 10^5, 10^7, or 10^9 CFU Δ*FTL1678*. On day 29 post-infection, mice were boosted with 10^9 CFU Δ*FTL1678* and animal health was monitored daily through day 50 post-infection. *** $P<0.001$; (B) Mice from A were intranasally-challenged with 120 CFU of wild-type SchuS4 [BSL3; 6× LD50]. Animal health was monitored daily through day 26 post-infection. *$P<0.001$

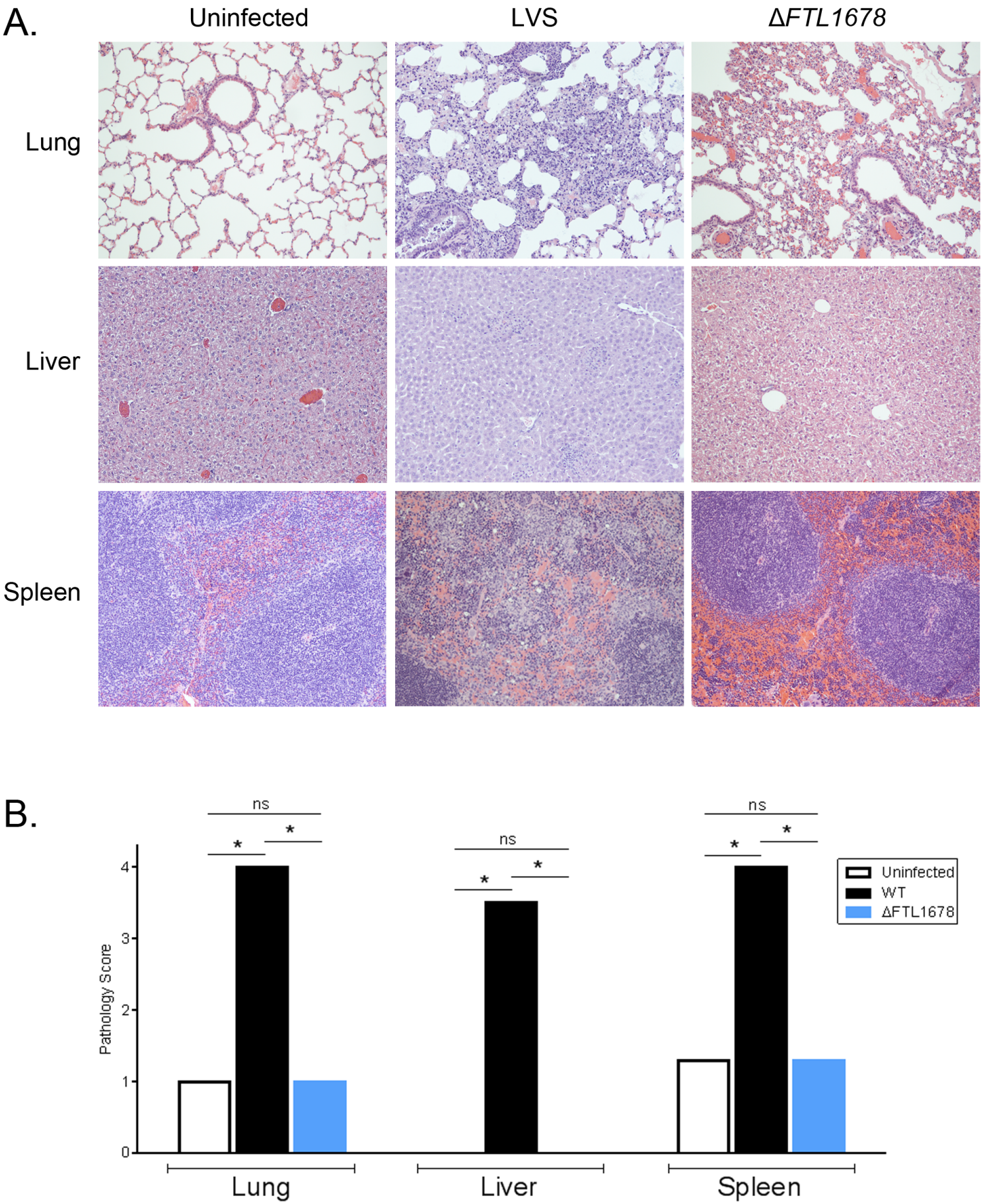

Fig 8. Δ*FTL1678* does not induce pathology. (A) Hematoxylin and eosin (H&E)-stained tissues were examined from either uninfected, *F. tularensis* WT LVS-, or Δ*FTL1678*-infected mice at 10× objective. (B) Tissues were graded on a scale of 0 to 4 with 4 being the most severe. *$P<0.05$